nature portfolio

Peer Review File

Harnessing chloride to drive catalyst reconstruction for durable and efficient seawater electrolysis

Corresponding Author: Professor Yingwei Li

This file contains all reviewer reports in order by version, followed by all author rebuttals in order by version.

Version 0:

Reviewer comments:

Reviewer #1

(Remarks to the Author)
While the authors present an extensive amount of experimental work, including operando spectroscopy, isotope labeling, and a 1.0 kW anion exchange membrane water electrolyzer (AEMWE) demonstration, this manuscript suffers from fundamental flaws in chemical engineering logic and physical chemistry mechanisms. The system's industrial viability and the proposed thermodynamic/kinetic models are highly questionable. Therefore, it does not meet the rigorous standards of Nature Communications.
1.Mixing 30 wt% KOH with seawater inevitably triggers massive Mg/Ca precipitation. The authors fail to explain how the AEMWE avoids rapid flow channel and porous layer clogging under such conditions.
2.The authors need to explicitly state whether the 30 wt% KOH + seawater mixture was filtered prior to AEMWE testing or not. If the precipitates were filtered out, the feed is merely an alkaline brine, not direct seawater. Meanwhile, if highly expensive 30 wt% pure KOH is required, industrial operators would simply use cheap RO-purified water instead of raw seawater, completely bypassing scaling and Cl- corrosion risks.
3.Highly soluble sulfate ions cannot stably anchor at the electrode interface for 7000 hours to repel Cl- under severe gas-scouring and strong convection at 1.0 A cm-2.
4.A 98% Faradaic efficiency for O2 is insufficient for industrial claims. At 1.0-2.0 A cm-2, severe local pH drops will thermodynamically favor the CER. The authors must provide highly sensitive, continuous quantitative tracking (e.g., UV-Vis or rigorous titration) of trace hypochlorite/chlorine, as even a 0.5% CER rate will rapidly degrade the system.
5.Using EXAFS fitting to claim precise atomic distance changes (from 3.15 Å to 2.96 Å) as the definitive proof of LOM to OPM transition is questionable. The reconstructed hydroxide layer is highly amorphous and dynamically evolving, making such precise static bond-length assignments highly ambiguous.
6.To substantiate the claim of stable 1.0 kW AEMWE operation, the authors should provide the differential pressure (inlet vs. outlet) curves over the 1500-hour test to prove the absence of flow channel clogging.
7.Provide low-magnification macroscopic photographs and large-area SEM images of the catalyst and membrane after the 7000-hour and AEMWE tests to demonstrate mechanical integrity and the absence of micro-scaling.
8.All Faradaic efficiency and mass activity measurements need to include rigorous error bars derived from multiple independent tests, which are currently lacking in some figures.

Reviewer #2

(Remarks to the Author)
This manuscript reports a sulfur-doped NiFe-MOF (NiFe-MOF-S) electrocatalyst designed for alkaline seawater electrolysis. The authors claim that the in situ generation of sulfate repels most chloride ions while allowing trace amounts to penetrate, which drives the structural reconstruction of the catalyst into a dense γ-NiFeOOH phase. This reconstruction is proposed to shift the oxygen evolution reaction (OER) mechanism from a lattice-oxygen-mediated (LOM) pathway to an oxide path mechanism (OPM), resulting in an impressively low overpotential of 213 mV at 500 mA cm-2 and a degradation rate of only 1.4 μV h-1 over 7000 hours at 1.0 A cm-2 in alkaline seawater.
The kilowatt-scale electrolyzer demonstration is highly commendable and application-oriented. On the other hand, the general concept of leveraging sulfate/polyanion layers to repel chloride in NiFe-based catalysts for seawater OER has been widely reported recently. If the author want to meet the novelty and mechanistic depth typically expected by this journal, stronger direct evidence for the "trace chloride" local concentration mechanism and the structural "density" of the

reconstructed phase are need to be provided
Overall, this study presents excellent engineering results but requires substantial strengthening of its mechanistic validation to avoid over-interpretation. Additional specific comments and suggestions are provided below:
1. Quantification of the “Trace Cl-” Mechanism: The core premise hinges on the claim that the sulfate layer allows “trace amounts of Cl-” to reach the metal sites to promote reconstruction. However, no experimental or theoretical quantification of this local chloride concentration is provided. How is the "trace" amount differentiated from total exclusion or severe penetration? The authors are encouraged to provide appropriate characterization to justify this specific interfacial mechanism.
2. Phase Density Over-interpretation: In Figure 3m, the authors use the Raman intensity ratio of δ(Ni-O) to v(Ni-O) (Iδ/v) to claim the formation of a “denser” γ-NiOOH phase in seawater compared to pure water. Relying solely on Raman peak intensity ratios to determine phase density is highly speculative, as these intensities are strongly influenced by surface roughness, laser focus, and sample orientation. Additional direct structural evidence, such as grazing-incidence XRD, is necessary to substantiate the claim of a denser structure.
3. Long-term Stability of the Protective Layer: Regarding the S 2p XPS analysis (Figure 1e), the authors assign peaks to M-S and S-O bonds. For a catalyst operating over 7000 hours, it is critical to understand the long-term stability of this sulfur species. Does the sulfide completely oxidize to dissolved sulfate over time? If so, how is the chloride-repelling layer maintained during the 7000-hour test. XPS spectra for the S 2p region after the 7000-hour test must be provided and discussed.
4. The author said that “the SEM images of NiFe-MOF-S/NF confirm that both the crystal structure and petal-like morphology of NiFe-MOF-S/NF are well preserved after long-term operation”, but this structure is no longer visible in Figure S28. The author should have been more precise in your description in the text.
5. The font size and style in each figure of the text should be made more uniform, for example, in Figure 2f.

Reviewer #3

(Remarks to the Author)
This manuscript reports a chloride-assisted catalyst reconstruction strategy to enhance activity and durability for alkaline seawater electrolysis using NiFe-MOF-derived catalysts. The authors demonstrate that trace amounts of Cl^- promote the formation of a dense γ-NiFeOOH phase, leading to improved OER activity and stability even at industrially relevant current densities. The work combines electrochemical measurements, operando spectroscopy, and DFT calculations, and the reported performance (e.g., 1.0 A cm^{-2} over 7000 h) is highly impressive.Overall, the topic is timely and important, and the combination of mechanistic insight (Fig. 3–4) and device-level demonstration (Fig. 5) makes the work potentially impactful. However, several key issues related to data interpretation, clarity of electrochemical analysis, and mechanistic justification need to be addressed before the manuscript can be considered for publication.I therefore recommend major revision.

Major comments
1. Unclear origin of Cl^--induced activity enhancement in single-metal systems
The authors report that even single-metal systems (Ni-MOF, Fe-MOF) show improved activity with increasing Cl^- concentration (page 7, lines 115–125) . However the explanation for this phenomenon is insufficient and largely speculative.The proposed mechanism based on dual-site regulation does not apply to single-metal systems.Fig. S4 does not clearly support the claimed trend, and the data presentation is not sufficiently clear to validate this conclusion.

Recommendation:Provide a clearer mechanistic explanation specifically for single-metal systems.
Include additional control experiments or discussion (e.g., surface reconstruction, conductivity, double-layer effects).
Improve clarity and readability of Fig. S4 (especially panel a and c).

2. Ambiguous peak assignment and spectroscopic interpretation
There are multiple issues regarding peak assignment:The assignments in page 9 (lines 139–140) are vague and lack justification. In the discussion around pages corresponding to lines 156–158, it is unclear which peaks are being referred to. Similar ambiguity appears in Raman/XAS discussions (Fig. 3 and related supplementary figures). These issues reduce confidence in the mechanistic conclusions.

Recommendation: Clearly indicate which peaks correspond to which chemical species in all figures.
Provide references or fitting details for peak assignments. Ensure consistency between main text and supplementary figures.

3. Inconsistency and insufficient explanation in LSV measurements
The manuscript states that LSV was measured at 5 mV s^{-1}, but the presence of reduction peaks (e.g., Fig. 2a) suggests that scans may have been performed in the negative direction (–5 mV s^{-1}). The origin of the reduction peaks is not explained when first introduced. The relationship between these peaks and catalyst reconstruction (Fig. 3j) is not clearly discussed.

Recommendation: Clarify scan direction and measurement protocol. Explicitly assign the reduction peaks (e.g., Ni2+/Ni3+ redox). Discuss how peak intensity relates to catalyst reconstruction and activity.

4. Insufficient treatment of error analysis and reproducibility
Error bars are missing or insufficiently described (e.g., Fig. 2c). There is no clear indication of repeatability or statistical

variation.

Recommendation: Include error bars for key electrochemical data. Provide number of replicates and standard deviations. Clarify whether the presented data are representative or averaged.

5. Questionable analysis of degradation rate (1.4 μV h^{-1})
The authors claim an ultralow degradation rate of 1.4 μV h^{-1} based on Fig. 2d/i . However, the potential profile clearly fluctuates over time. It is unclear how this value was extracted.
Given the noise level, the significance of 1.4 μV h^{-1} is questionable.

Recommendation: Provide a detailed method for calculating degradation rate (e.g., linear fitting window). Include statistical uncertainty. Discuss whether the fluctuation level allows meaningful extraction of such a small value.

6. Insufficient evidence for correlation between Cl^- concentration, reduction peak, and activity
In Fig. 3, the authors suggest a correlation between: Cl^- concentration, Reduction peak intensity,
and OER activity. However, no quantitative correlation analysis is provided. The causality remains unclear.

Recommendation: Provide quantitative correlation (e.g., peak current vs activity).Consider additional experiments (e.g., controlled CV cycles, operando tracking).

Finally, the mechanistic insight (Fig. 4) and performance (Fig. 5) are highly significant and could make this work suitable for publication in a high-impact journal. However, the current manuscript contains several issues in data interpretation, electrochemical analysis, and clarity.

I recommend publication after major revision addressing the points above.

Reviewer #4

(Remarks to the Author)
This work proposes a strategy to regulate the flux of chloride ions near the catalytic sites during seawater electrolysis. Sulfur species generate sulfate in situ to repel most Cl^- while allowing a small amount of chloride to remain and promote catalyst reconstruction. As a result, the catalyst reconstructs into a dense γ-NiFeOOH phase with shortened Ni–Fe bond lengths, which improves the OER activity and stability in alkaline seawater. A series of electrochemical measurements and operando characterizations are provided to support the proposed mechanism. Some technical issues need to be addressed before further consideration of this work.
1. The structural description of the catalyst needs clarification. The manuscript refers to sulfur-doped NiFe nanoparticles, while Fig. 1 suggests the formation of NiS2 nanoparticles. It should be clarified whether sulfur is present as dopants or forms a separate sulfide phase.
2. The structural analysis in Fig. 3 mainly focuses on the catalyst after the OER test. To clearly demonstrate the reconstruction process, a direct comparison between the catalyst before and after OER should be provided.
3. The Raman data in Fig. 1d are not very convincing. The spectral quality is relatively poor, and the assignment of the additional peaks is too general, as they are simply attributed to M–S vibrations without sufficient explanation.
4. Although the manuscript reports electrolyser performance, the experimental section does not include any description of the electrolyser testing.
5. The in situ ATR-SEIRAS spectra in Fig. 4a–b are not very convincing due to the relatively weak signal intensity and poorly resolved spectral features.
6. The authors should provide more details regarding the industrial electrolyzer tests. In particular, post-test characterization of the electrodes (e.g., morphology and structural analysis) is needed to explain the excellent stability observed during long-term operation.
7. The techno-economic analysis relies on several assumptions that are insufficiently justified, such as the electricity price (0.02 $/kWh), electrolyser capital cost (450 $/kW), capacity factor (0.9), and catalyst/membrane cost (5% of electrolyser cost). These parameters appear overly optimistic and are not adequately supported by references.

Version 1:

Reviewer comments:

Reviewer #1

(Remarks to the Author)
The authors have well addressed the concerns of the reviewers. Now it is ready for publication.

Reviewer #2

(Remarks to the Author)
The revised version has satisfactorily addressed all points raised in the previous review round. No further changes are

needed. I recommend acceptance.

Reviewer #3

(Remarks to the Author)
The authors have satisfactorily addressed my major comments through additional analyses, control experiments, and clarifications. While some mechanistic interpretations may remain open to discussion, the authors have provided reasonable supporting evidence and appropriate literature precedents. I therefore consider my previous concerns to be adequately resolved.

Reviewer #4

(Remarks to the Author)
The authors made good response to my previous concerns, I am supportive of the acceptance of this manuscript in current form.

Responses to reviewer #1:

While the authors present an extensive amount of experimental work, including operando spectroscopy, isotope labeling, and a 1.0 kW alkaline seawater electrolyzer (ASWE) demonstration, this manuscript suffers from fundamental flaws in chemical engineering logic and physical chemistry mechanisms. The system's industrial viability and the proposed thermodynamic/kinetic models are highly questionable. Therefore, it does not meet the rigorous standards of *Nature Communications*.

Response: We sincerely thank the reviewer for the insightful and constructive comments. In response to the reviewer's concerns regarding the chemical engineering logic and physical chemistry mechanisms, we conducted additional experiments and characterizations. These new results further support our conclusions and reinforce the industrial applicability and feasibility of the proposed system.

Specifically: (1) We clarified the electrolyte pretreatment procedure, including centrifugation to remove Mg/Ca precipitates, and provided system pressure monitoring data demonstrating that no clogging occurred in the 1.0 kW ASWE during 1500 hours of operation. (2) We provided UV-vis absorption spectra of ClO^- to verify the high selectivity toward OER, even at high current densities. (3) We added post-test SEM and XPS analyses to demonstrate the morphological of the catalyst and chemical stability of the anchored sulfate species after 7000 hours of laboratory-scale measurement and 1500 hours of 1.0 kW-scale ASWE operation. (4) We replicated measurements for key electrochemical performance and Faradaic efficiency data and included error bars to improve the reliability and reproducibility of the results. (5) We further validated the proposed OPM mechanism through a comprehensive analysis combining EXAFS, in situ ATR-SEIRAS, ^{18}O-labeled DEMS, and DFT calculations.

With these revisions, we believe the manuscript now presents a robust and comprehensive demonstration of both the fundamental mechanism and practical applicability of our Cl^--driven catalyst reconstruction strategy for durable seawater electrolysis. We hope the reviewer will find the revised manuscript significantly improved and suitable for publication in *Nature Communications*.

1.Mixing 30 wt% KOH with seawater inevitably triggers massive Mg/Ca precipitation. The authors fail to explain how the ASWE avoids rapid flow channel and porous layer clogging under such conditions.

Response: We sincerely thank the reviewer for the valuable comment. The mixture of 30 wt% KOH with seawater was subjected to centrifugation to remove the Mg/Ca precipitation prior to ASWE testing, thereby preventing the clogging of flow channels and porous layers during long-term operation. Such pretreatment, involving alkaline precipitation followed by filtration or centrifugation to remove Mg/Ca species, is widely adopted in seawater electrolysis to prevent physical blockage during operation (e.g., *Sci. Adv.* **9**, eadi7755 (2023); *Nat. Rev. Mater.* **10**, 857–873 (2025); *Nat. Commun.* **15**, 10351 (2024); *Angew. Chem. Int. Ed.* **62**, e202311674 (2023)). We have included the detailed procedures in the revised main text (lines 627–629 of page 35).

2.The authors need to explicitly state whether the 30 wt% KOH + seawater mixture was filtered prior to ASWE testing or not. If the precipitates were filtered out, the feed is merely an alkaline brine, not direct seawater. Meanwhile, if highly expensive 30 wt% pure KOH is required, industrial operators would simply use cheap RO-purified water instead of raw seawater, completely bypassing scaling and Cl- corrosion risks.

Response: We sincerely thank the reviewer for this comment. In this study, the mixture of 30 wt% KOH + seawater was centrifuged prior to testing to remove $Mg(OH)_2$ and $Ca(OH)_2$ precipitates. This pretreatment enabled the evaluation of the intrinsic OER activity and Cl^- corrosion resistance of the catalyst without interference from physical blockage effects. Many studies on seawater electrolysis similarly remove Mg^{2+}/Ca^{2+} precipitates from alkalize seawater through filtration or centrifugation prior to electrolysis (e.g., *Sci. Adv.* **9**, eadi7755 (2023); *Nat. Rev. Mater.* **10**, 857–873 (2025); *Nat. Commun.* **15**, 10351 (2024); *Angew. Chem. Int. Ed.* **62**, e202311674 (2023)). We agree with the reviewer that, after removal of $Mg(OH)_2$ and $Ca(OH)_2$ precipitates, the electrolyte is technically more accurately described as an alkaline brine rather than raw

seawater. However, we note that many studies in the field of seawater electrolysis still use the term "KOH + seawater" to describe the electrolyte system, in order to distinguish the use of seawater-derived feedstocks from pure water systems (e.g., *Nat. Commun.* **15**, 10351 (2024); *Angew. Chem. Int. Ed.* **62**, e202311674 (2023); *Nat Commun.* **15**, 2481 (2024); *Nano Energy* **98**, 107295 (2022); *Appl. Catal. B-Environ.* **342**, 123376 (2024); *Appl. Catal. B-Environ.* 338, 122996 (2023); *J. Energy Chem.* **75**, 66–73 (2022); *Nano Energy* 111987 (2026)). The remaining Cl^- species represent the primary corrosive component and constitute the major challenge in seawater electrolysis. The focus of this work is to investigate the beneficial role of Cl^- in promoting catalyst reconstruction and inducing the OER mechanism transition, rather than addressing the engineering challenges associated with precipitate removal. For practical applications, simple methods strategies, such as mechanical scraping of the electrode surface, can be employed to remove any residual deposits. However, addressing these engineering aspects is beyond the scope of this fundamental study. Nevertheless, as suggested by the reviewer, we have explicitly clarified in the revised manuscript that the electrolyte used in this study is precipitation-treated seawater (lines 627–629 of page 35).

Furthermore, we agree that using RO-purified water can bypass scaling and Cl^- corrosion risks. In a large-scale centralized facility, seawater desalination via RO can achieve relatively low unit cost owing to economies of scale. The key advantage of using raw seawater instead of RO-purified water lies in its suitability for distributed hydrogen production scenarios. For distributed applications, such as offshore wind-powered electrolysis across multiple platforms, hydrogen supply on remote islands, or coastal hydrogen refueling stations, installing dedicated RO systems at each small-scale site would result in increased capital investment, energy consumption, footprint requirements, and maintenance costs per unit of hydrogen produced (e.g., *Sci. Bull.* **71**, 172–195 (2026); *Nat. Rev. Clean Technol.* **2**, 305–319 (2026); *Nat. Rev. Mater.* **10**, 857–873 (2025)). In such distributed scenarios, seawater electrolysis with simple pretreatment methods (e.g., sedimentation) offers a practical and attractive solution by

directly utilizing locally available seawater and renewable energy sources without requiring extensive water purification infrastructure. We have included related references (Ref. 5 and 6) and added related discussion in the revised main text (lines 41–43 of page 4).

3.Highly soluble sulfate ions cannot stably anchor at the electrode interface for 7000 hours to repel Cl^- under severe gas-scouring and strong convection at 1.0 A cm^{-2}.

Response: We sincerely thank the reviewer for this valuable comment. We agree with the reviewer that free SO_4^{2-} ions would be readily removed under conditions of vigorous gas evolution and electrolyte convection. However, in our system, the sulfate species do not exist as free ions; instead, they are anchored on the catalyst surface through interactions with metal active sites. To directly address the reviewer's concern regarding long-term stability, we performed XPS characterization of the NiFe-MOF-S catalyst after 7000 hours of operation at 1.0 A cm^{-2} in alkaline seawater. The S 2p spectrum clearly exhibits characteristic peaks corresponding to the S–O bonds of SO_4^{2-} species (Supplementary Fig. S32), confirming that SO_4^{2-} species remain at the electrode interface even after prolonged operation under industrially relevant conditions. This observation is consistent with recent reports in which surface-bound sulfate species remained detectable by XPS even after thousands of hours of electrolysis (e.g., *Nat. Commun.* **17**, 3014 (2026); *Adv. Funct. Mater.* **35**, 2419871 (2025); *Appl. Catal. B: Environ. Energy* **381**, 125897 (2026)), confirming that SO_4^{2-} species can be stably anchored through coordination interactions with metal sites. Furthermore, the stable presence of the SO_4^{2-} protective layer may be attributed to the directional migration and preferential adsorption of sulfate species onto the anode surface under the applied electric field. In addition, the high chemical and electrochemical stability of SO_4^{2-} renders it resistant to oxidation under anodic operating potentials (e.g., *Angew. Chem. Int. Ed.* **60**, 22740–22744 (2021)).

Additionally, to determine whether externally introduced sulfate species could provide similar protection, we conducted a control experiment using NiFe-MOF/NF

(without sulfide) in alkaline seawater supplemented with 0.05 M Na_2SO_4. As shown in Supplementary Fig. S33, this electrode maintained stable operation for only approximately 230 h at 1.0 A cm^{-2}, after which rapid performance degradation was observed. This result supports the reviewer's concern that freely dissolved SO_4^{2-} species cannot stably retained or anchored on the catalyst surface during prolonged operation. In contrast, the sulfate species generated *in situ* from NiFe-MOF-S/NF remain firmly anchored through metal–SO_4^{2-} coordination, thereby providing sustained Cl^- repulsion and enabling stable operation for up to 7000 h. The XPS spectrum and control experiment results have been added into the revised manuscript to further support the long-term stability and anchoring behavior of the sulfate species (line 231 of page 13 to line 238 of page 14).

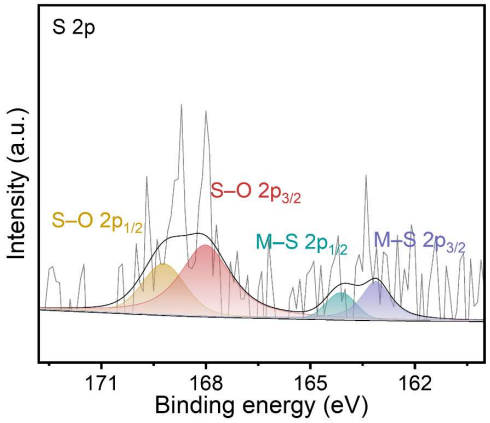

Fig. S32. XPS spectrum of S 2p for NiFe-MOF-S after 7000-h durability test at 1.0 A cm^{-2} in 1 M KOH + seawater.

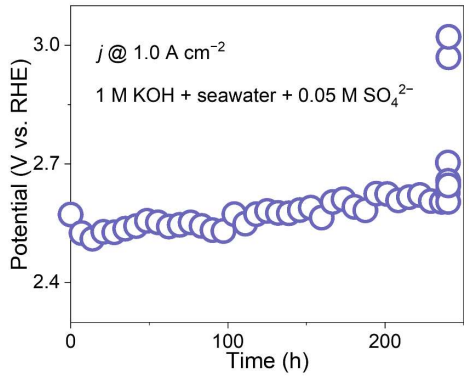

Fig. S33. OER durability test at 1.0 A cm^{-2} for NiFe-MOF/NF in 1 M KOH + seawater with 0.05 M Na_2SO_4.

4.A 98% Faradaic efficiency for O_2 is insufficient for industrial claims. At 1.0-2.0 A cm^{-2}, severe local pH drops will thermodynamically favor the CER. The authors must provide highly sensitive, continuous quantitative tracking (e.g., UV-Vis or rigorous titration) of trace hypochlorite/chlorine, as even a 0.5% CER rate will rapidly degrade the system.

Response: We sincerely thank the reviewer for this valuable comment. To verify the occurrence of the chlorine evolution reaction (CER), we performed UV-vis absorption spectroscopy using DPD (N,N-diethyl-p-phenylenediamine) to detect ClO^- species in the electrolyte after stability tests at 1.0 A cm^{-2}. The absorbance signals corresponding to ClO^- were negligible in the electrolyte after the stability tests (Supplementary Fig. S27), confirming the high OER selectivity of NiFe-MOF-S/NF even after prolonged operation. This observation is consistent with recent reports on high-performance seawater electrolysis catalysts, in which FE values of approximately 98–99% were achieved without detectable ClO^- formation (e.g., *ACS Nano* **19**, 31598–31608 (2025); *Adv. Mater.* **38**, e13754 (2026); *Nat. Commun.* **16**, 3098 (2025)). Therefore, the observed FE for O_2 being slightly lower than 100% is likely attributable to experimental uncertainties associated with the gas collection method, such as manual reading errors. The UV–vis absorption measurements of the post-reaction electrolyte have been included in the revised Supporting Information, and the corresponding discussion has been incorporated into the revised manuscript (lines 222–225 of page 13).

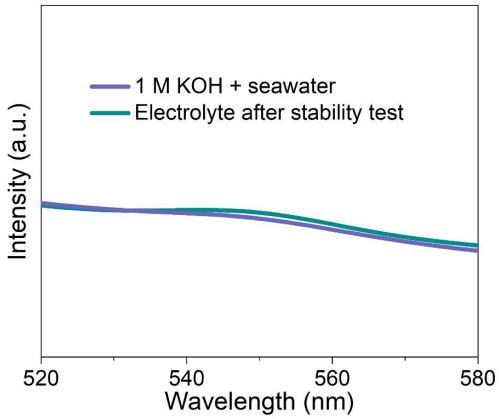

Fig. S27. UV-vis absorption spectra of electrolyte after stability tests with DPD.

5.Using EXAFS fitting to claim precise atomic distance changes (from 3.15 Å to 2.96 Å) as the definitive proof of LOM to OPM transition is questionable. The reconstructed hydroxide layer is highly amorphous and dynamically evolving, making such precise static bond-length assignments highly ambiguous.

Response: We sincerely thank the reviewer for this constructive comment. We agree with the reviewer that the reconstructed γ-NiFeOOH layer is amorphous and dynamically evolving. We also acknowledge that relying solely on EXAFS-derived bond length variations would not provide sufficient evidence to conclusively establish the OPM mechanism. Accordingly, we adopted a multi-technique approach to substantiate our mechanistic conclusions by integrating EXAFS analysis with complementary in situ spectroscopic evidence, electrochemical characterization, and DFT calculations.

First, the use of EXAFS to probe changes in metal–metal (M–M) distances in electrocatalysts is well established. Several recent studies have similarly employed EXAFS to correlate shortened M–M distances with the activation of the OPM pathway, thereby providing quantitative references for mechanistic interpretation (*J. Am. Chem. Soc.* **145**, 7829–7836 (2023); *Angew. Chem. Int. Ed.* e8854134 (2026); *Appl. Catal. B: Environ.* **354**, 124114 (2024); *Adv. Mater.* **38**, e72241 (2026); *J. Am. Chem. Soc.* **147**, 34169–34180 (2025); *Adv. Funct. Mater.* **36**, e16646 (2026)). In our study, the EXAFS

analysis revealed a contraction of the Ni–Fe bond distance from 3.15 Å in alkaline water to 2.96 Å in alkaline seawater, consistent with the formation of a more compact γ-NiFeOOH phase.

To further provide direct experimental evidence supporting the OPM mechanism, we performed in situ ATR-SEIRAS and ^{18}O-labeled DEMS measurements. As shown in Fig. 4a and Table S3, a distinctive absorption peak at 1104 cm^{-1}, corresponding to the *O–O* stretching vibration, was observed in alkaline seawater. This feature is characteristic of the oxygen bridge intermediate (M–O–O–M) formed during the OPM pathway (e.g., *Energy Environ. Sci.* **13**, 2200–2208 (2020); *Chem.* **7**, 2101–2117 (2021); *Proc. Natl. Acad. Sci. U.S.A.* **121**, e2317247121 (2024); *Nat. Catal.* **4**, 1012–1023 (2021); *J. Am. Chem. Soc.* **145**, 7829–7836 (2023); *Nat. Commun.* **15**, 95 (2024); *Joule* **10**, 2542–4351 (2026)). In contrast, this feature was absent in alkaline water. Furthermore, DEMS analysis revealed a significantly higher $^{36}O_2/^{34}O_2$ signal ratio in alkaline seawater, which was 15.9 times greater than that observed in alkaline water. These results confirm the suppression of lattice oxygen participation and indicate that the OER preferentially proceeds via the OPM pathway (Fig. 4f). Similar DEMS observations have also been reported in previous studies investigating the OPM mechanism, further supporting our mechanistic interpretation (e.g., *Nat. Catal.* **4**, 1012–1023 (2021); *Adv. Energy Mater.* e06195 (2026); *Adv. Mater.* e21163 (2026); *Joule* **10**, 2542–4351 (2026); *Nat. Commun.* **16**, 8145 (2025)).

DFT calculations further corroborate this mechanistic transition. As shown in Figs. 4j–4k and Supplementary Figs. S63 and S64, the calculated free energy barriers for the rate-determining step on compact S-NiFeOOH, featuring a shortened Ni–Fe bond length, is 1.72 eV for the OPM pathway. This value is substantially lower than those calculated for the AEM (3.22 eV) and LOM (2.93 eV) pathways. In contrast, for the conventional L-NiFeOOH with longer Ni–Fe bonds distances, the LOM pathway is energetically most favorable, exhibiting the lowest free energy barrier of 1.9 eV. These theoretical results confirm that the Cl^--induced formation of S-NiFeOOH with shortened Ni–Fe bonds distances favor the OPM pathway, thereby enhancing both the

intrinsic catalytic activity and long-term durability.

Therefore, the EXAFS-derived bond length contraction provides structural evidence for the formation of a more compact γ-NiFeOOH phase, and the mechanistic transition from LOM to OPM is established collectively through the combined evidence from in situ vibrational spectroscopy, isotopic DEMS measurements, DFT calculations, and pH-dependent OER analyses.

6.To substantiate the claim of stable 1.0 kW ASWE operation, the authors should provide the differential pressure (inlet vs. outlet) curves over the 1500-hour test to prove the absence of flow channel clogging.

Response: We sincerely thank the reviewer for the constructive suggestion. Our kW-scale ASWE system was not equipped with pressure transducers at the inlet and outlet; therefore, differential pressure data could not be obtained. However, the overall system pressure was monitored throughout the 1500 h operation and remained stable at approximately 0.1 MPa (Supplementary Fig. S66), indicating no significant increase in flow resistance occurred due to channel clogging. Moreover, after the 1500-hour test, the electrolyzer was disassembled, and visual inspection revealed no observable signs of clogging (Supplementary Fig. S67). Additionally, we note that the stable cell voltage maintained throughout the entire 1500 h operation provides indirect evidence that no significant flow channel clogging occurred, as clogging would typically lead to a gradual increase in cell voltage owing to enhanced mass transport resistance (Fig. 5h). Additionally, the electrolyte was pretreated by centrifugation to remove Mg/Ca precipitates prior to operation, thereby minimizing the risk of scaling accumulation. We have provided the pressure curve (Supplementary Fig. S66), post-test photographs of the disassembled 1.0 kW ASWE (Supplementary Fig. S67), and added related discussion in the revised manuscript (lines 488–492 of page 29).

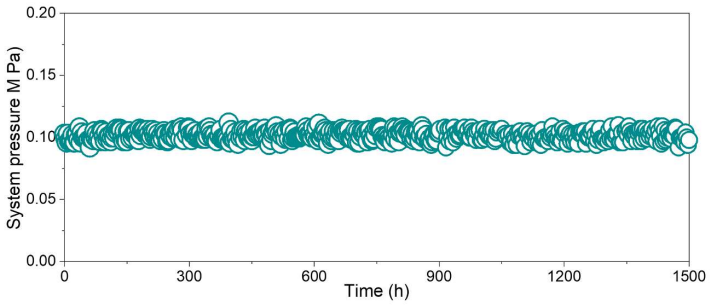

Fig. S66. System pressure of the 1.0 kW-scale ASWE for 1500-hour operation.

Fig. S67. Post-test photographs of the disassembled 1.0 kW ASWE showing the bipolar plate with three ports (electrolyte inlet/outlet, O_2 outlet, and H_2 outlet) after operation.

7. Provide low-magnification macroscopic photographs and large-area SEM images of the catalyst and membrane after the 7000-hour and ASWE tests to demonstrate mechanical integrity and the absence of micro-scaling.

Response: We sincerely thank the reviewer for this valuable suggestion. To demonstrate the mechanical integrity of the catalyst and confirm the absence of microscale deposits, we have provided SEM images of the NiFe-MOF-S/NF catalyst after both the 7000-hour stability test and the ASWE operation. As shown in Supplementary Figs. S31 and S68, the catalyst retains a flake-like morphology after long-term operation, confirming its excellent structural stability. These observations are consistent with the stable electrochemical performance presented in Fig. 2d and Fig. 5h. These SEM images and the corresponding discussion have been incorporated into the revised manuscript (lines 229–231 of page 13 and lines 492–493 of page 29).

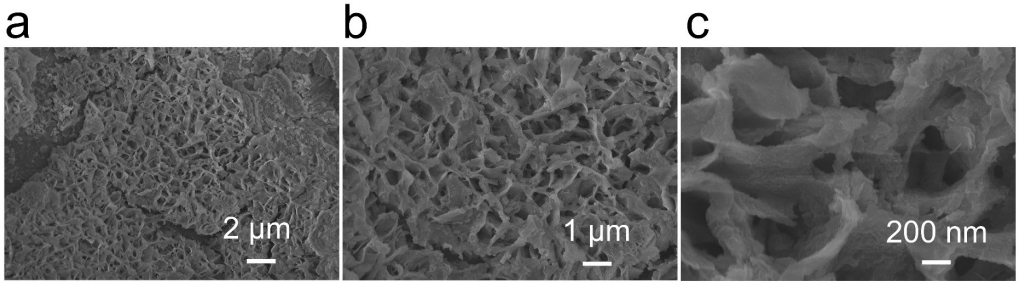

Fig. S31. SEM images of NiFe-MOF-S/NF after 7000-hour durability test in 1 M KOH + seawater.

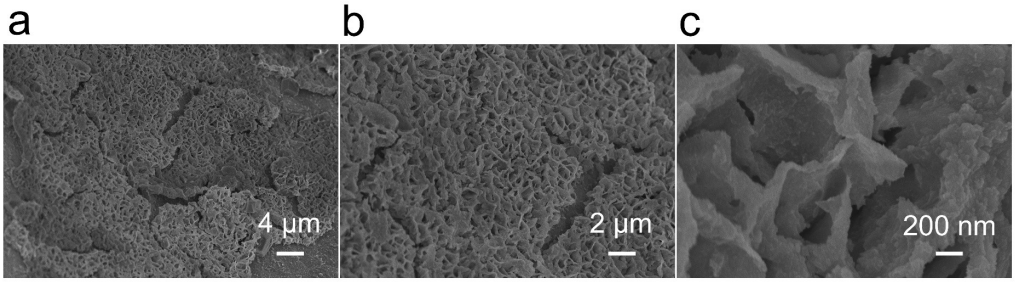

Fig. S68. SEM images of NiFe-MOF-S/NF after durability test in a 1.0 kW-scale ASWE.

8.All Faradaic efficiency and mass activity measurements need to include rigorous error bars derived from multiple independent tests, which are currently lacking in some figures.

Response: We thank the reviewer for this constructive suggestion. To address the reviewer's concerns regarding error analysis and reproducibility, we have added error bars to all Faradaic efficiency measurements based on three independent tests. The results show that the Faradaic efficiency for oxygen evolution remains as high as 99% under the tested conditions (Supplementary Fig. S29), demonstrating the excellent OER selectivity of the catalyst. Additionally, error bars have been incorporated for key electrochemical parameters, including the activation energy values derived from Arrhenius analysis. The Arrhenius analysis based on temperature-dependent OER activity reveals that the activation energy of NiFe-MOF-S/NF decreases from 40.9 kJ

mol^{-1} in alkaline water to 25.2 kJ mol^{-1} in alkaline seawater. These revisions have been incorporated into the updated figures (e.g., Fig. 2c and Supplementary Fig. S29), along with the corresponding discussion in the main text (lines 201–204 of page 12 and lines 225–227 of page 13).

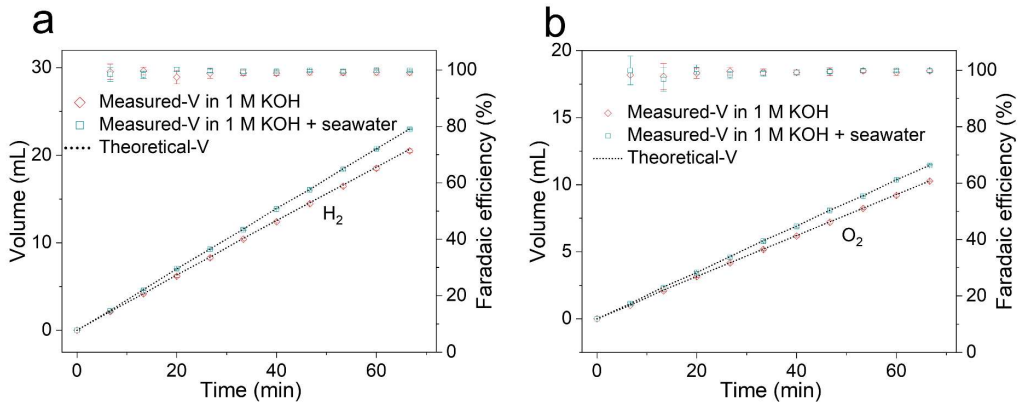

Fig. S29. The produced (a) H_2 and (b) O_2 quantity during overall splitting of NiFe-MOF-S/NF in 1 M KOH and 1 M KOH + seawater.

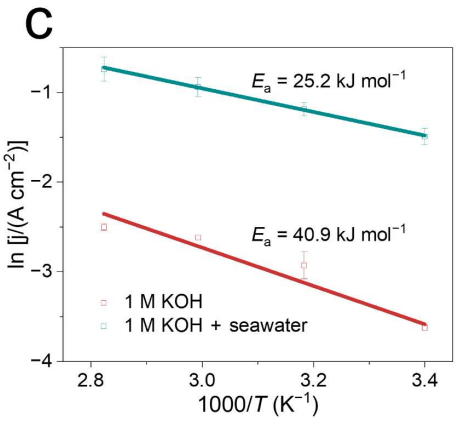

Fig. 2. (c) Arrhenius plot of NiFe-MOF-S/NF at 1.4 V vs. RHE in 1 M KOH and 1 M KOH + seawater.

Responses to reviewer #2:

This manuscript reports a sulfur-doped NiFe-MOF (NiFe-MOF-S) electrocatalyst designed for alkaline seawater electrolysis. The authors claim that the in situ generation of sulfate repels most chloride ions while allowing trace amounts to penetrate, which drives the structural reconstruction of the catalyst into a dense γ-NiFeOOH phase. This reconstruction is proposed to shift the oxygen evolution reaction (OER) mechanism from a lattice-oxygen-mediated (LOM) pathway to an oxide path mechanism (OPM), resulting in an impressively low overpotential of 213 mV at 500 mA cm^{-2} and a degradation rate of only 1.4 μV h^{-1} over 7000 hours at 1.0 A cm^{-2} in alkaline seawater. The kilowatt-scale electrolyzer demonstration is highly commendable and application-oriented. On the other hand, the general concept of leveraging sulfate/polyanion layers to repel chloride in NiFe-based catalysts for seawater OER has been widely reported recently. If the author want to meet the novelty and mechanistic depth typically expected by this journal, stronger direct evidence for the "trace chloride" local concentration mechanism and the structural "density" of the reconstructed phase are need to be provided. Overall, this study presents excellent engineering results but requires substantial strengthening of its mechanistic validation to avoid over-interpretation.

Response: We sincerely thank the reviewer for the positive evaluation and recognition of our work. To further substantiate this claim and directly address the reviewer's specific concerns, we have provided the following additional evidence:

Quantification of the "trace Cl^-" mechanism: We systematically compared the performance of unprotected catalysts (Ni-MOF, Fe-MOF, and NiFe-MOF) with that of the optimally protected catalyst (NiFe-MOF-S) in electrolytes with different concentration of Cl^-. The volcano-shaped activity trend confirms that trace Cl^- intrinsically promotes the OER, while the sulfate layer regulates the local Cl^- concentration to maintain it within this optimal "trace" range.

Structural density of the reconstructed phase: We use EXAFS-derived Ni–Fe bond distance (from 3.15 Å to 2.93 Å) as the primary structural evidence for the formation

of a denser γ-NiFeOOH phase, while the Raman $I_{\delta/\nu}$ ratio serves as complementary supporting evidence. Literature references have been cited to further validate the correlation between Raman peak intensity ratios and structural compactness.

All issues raised by the reviewer have been carefully addressed in the point-by-point responses provided below. We believe that the revised manuscript now provides the necessary mechanistic insight and scientific novelty to meet the standards for publication in *Nature Communications*.

Additional specific comments and suggestions are provided below:

1. Quantification of the "Trace Cl^-" Mechanism: The core premise hinges on the claim that the sulfate layer allows "trace amounts of Cl^-" to reach the metal sites to promote reconstruction. However, no experimental or theoretical quantification of this local chloride concentration is provided. How is the "trace" amount differentiated from total exclusion or severe penetration? The authors are encouraged to provide appropriate characterization to justify this specific interfacial mechanism.

Response: We sincerely thank the reviewer for this valuable comment. To distinguish the effects of "trace" Cl^- exposure from complete exclusion or excessive penetration, we systematically compared the behavior of catalysts without sulfide protection (Ni-MOF/NF, Fe-MOF/NF, and NiFe-MOF/NF) with that of the optimally sulfide-protected catalyst (NiFe-MOF-S/NF) in electrolytes with different concentration of Cl^-.

Without sulfide protection: Ni-MOF/NF, Fe-MOF/NF, and NiFe-MOF/NF all exhibit a volcano-shaped OER activity trend with increasing Cl^- concentration (0–2 M NaCl in 1 M KOH), achieving optimal performance in 1 M KOH + 0.05 M NaCl (Supplementary Fig. S5). To further investigate the promotional effect of trace Cl^-, we performed CV tests for Ni-MOF/NF and Fe-MOF/NF in 1 M KOH, 1 M KOH + 0.05 M NaCl, and 1 M KOH + 0.5 M NaCl (Supplementary Figs. S46 and S47). For both catalysts, the reduction peak current density is higher in 1 M KOH + 0.05 M NaCl than that in 1 M KOH, indicating increased degree of structural transformation. In contrast, at 0.5 M Cl^-, the catalysts show lower reduction peak current densities due to excessive

Cl^--induced corrosion. These results directly demonstrate that a low Cl^- concentration (0.05 M) promotes surface reconstruction and enhances OER activity, whereas higher Cl^- concentrations lead to severe corrosion and performance degradation.

With optimal sulfide protection (NiFe-MOF-S/NF): The in situ-generated SO_4^{2-} layer functions as a selective protective barrier. Consequently, NiFe-MOF-S/NF maintains high OER activity even in alkaline seawater containing ~0.5 M Cl^-, without the activity drop observed for the unprotected catalyst (Fig. 2a, and Supplementary Figs. S4 and S5). This result indicates that the sulfate layer suppresses excessive Cl^- penetration while still allowing a limited amount of Cl^- to reach the metal surface and promote catalyst reconstruction. The optimal NiS_2 loading balances protection and promotion effects. Insufficient sulfide loading results in severe Cl^--induced corrosion (NiFe-MOF-S-0.5/NF), whereas excessive sulfide loading completely blocks Cl^- access, thereby suppressing its beneficial promotional effect (NiFe-MOF-S-1.5/NF) (Supplementary Fig. S10).

To dynamically distinguish beneficial "trace" penetration from severe corrosion, we performed current–time (i–t) measurements at 1.64 V vs. RHE in both 1 M KOH and 1 M KOH + seawater electrolytes (Supplementary Fig. S48). For NiFe-MOF-S/NF, the current density obtained in 1 M KOH + seawater is higher than that in 1 M KOH, indicating that the trace amount of Cl^- penetrating the sulfate layer promotes surface reconstruction and enhances OER kinetics. In sharp contrast, for NiFe-MOF/NF, the current density in 1 M KOH + seawater is not only lower than that in pure 1 M KOH but also continuously decreases with time, indicating severe Cl^--induced corrosion and active-site poisoning. This result directly demonstrates that the sulfate layer permits only a beneficial "trace" amount of Cl^- to penetrate and participate in catalyst reconstruction, whereas unprotected catalysts are subjected to severe Cl^- attack and consequent performance degradation.

Thus, the "trace" Cl^- exposure is experimentally defined as the amount of Cl^- reaching the metal surface under optimal sulfate coverage, which is sufficient to promote catalyst reconstruction, as evidenced by enhanced Ni oxidation and Ni–Fe

bond length contraction, yet insufficient to induce corrosion, as demonstrated by low metal leaching and excellent long-term stability. The volcano-shaped activity trend observed for the unprotected catalysts confirms that trace amounts of Cl^- are intrinsically beneficial for OER enhancement, while the sulfate layer regulates the local Cl^- concentration to maintain this optimal "trace" level even under high-Cl^- seawater conditions. We have included the new catalytic results in Supplementary Figs. S5 and S46 and added related discussion in the revised manuscript (lines 117–119 of page 7 and from line 318 of page 18 to line 337 of page 19).

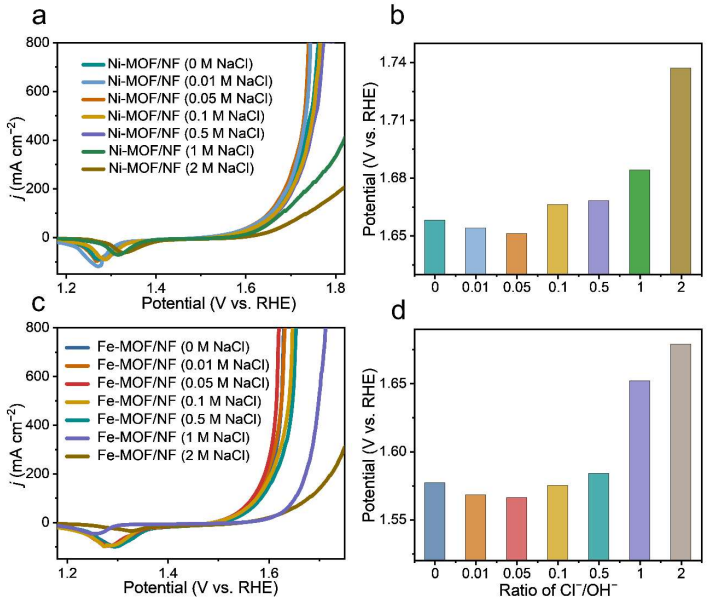

Fig. S5. (a, c) The LSV polarization curves for (a) Ni-MOF/NF and (c) Fe-MOF/NF in electrolytes with different Cl^-/OH^- ratios in 1 M KOH. (b, d) Comparison of overpotentials for (b) Ni-MOF/NF and (d) Fe-MOF/NF at a current density of 100 mA cm^{-2}.

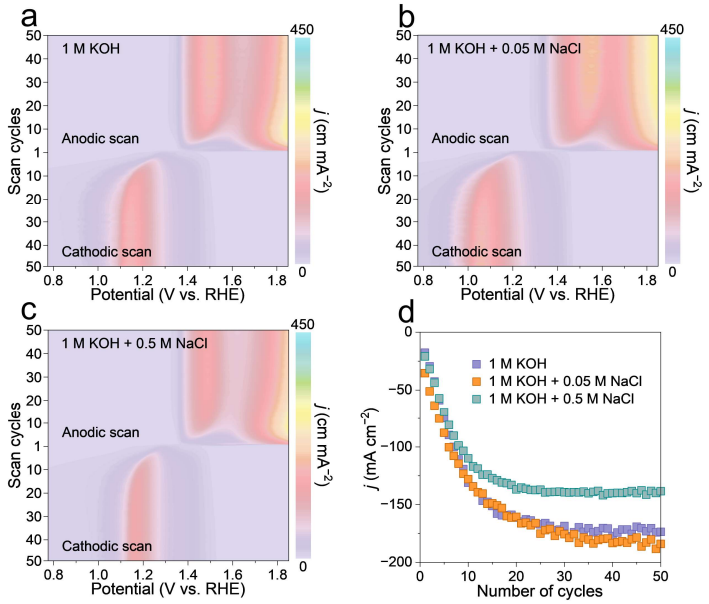

Fig. S46. (a, b, c) The evolution of CV curves for Ni-MOF/NF from the 1st to the 50th cycle in (a) 1 M KOH, (b) 1 M KOH + 0.05 M NaCl, and (c) 1 M KOH + 0.5 M NaCl at 20 mV s^{-1} between 0.774 and 1.85 V vs. RHE. (d) The variation of reduction peak current density with CV cycles for Ni-MOF/NF in 1 M KOH, 1 M KOH + 0.05 M NaCl, and 1 M KOH + 0.5 M NaCl.

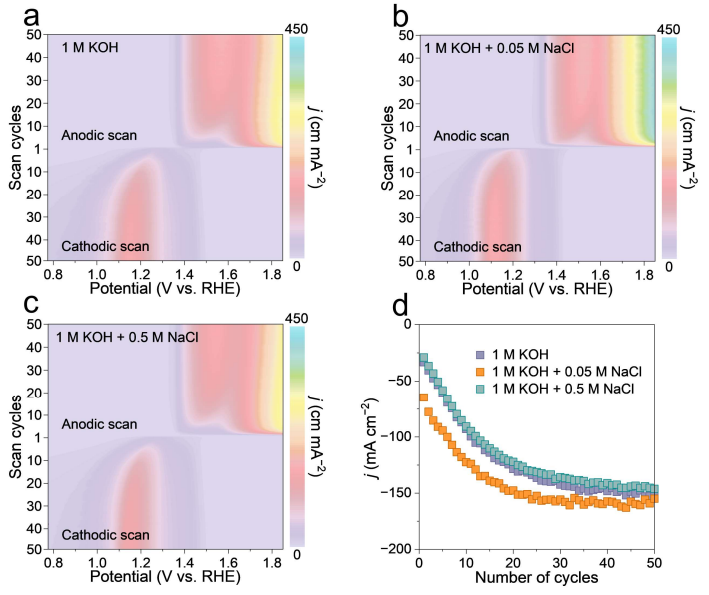

Fig. S47. (a, b, c) The evolution of CV curves for Fe-MOF/NF from the 1st to the 50th cycle in (a) 1 M KOH, (b) 1 M KOH + 0.05 M NaCl, and (c) 1 M KOH + 0.5 M NaCl

at 20 mV s^{-1} between 0.774 and 1.85 V vs. RHE. (d) The variation of reduction peak current density with CV cycles for Fe-MOF/NF in 1 M KOH, 1 M KOH + 0.05 M NaCl, and 1 M KOH + 0.5 M NaCl.

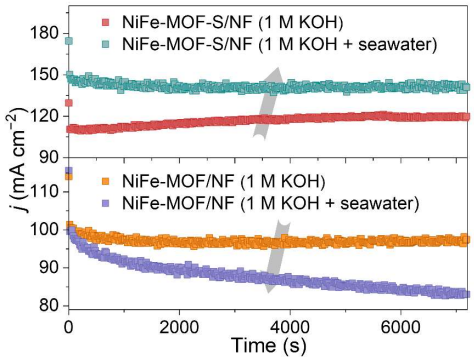

Fig. S48. I–t curves of NiFe-MOF/NF and NiFe-MOF-S/NF in 1 M KOH and 1 M KOH + seawater at 1.64 V vs. RHE.

2. Phase Density Over-interpretation: In Figure 3m, the authors use the Raman intensity ratio of δ(Ni-O) to ν(Ni-O) ($I_{\delta/\nu}$) to claim the formation of a "denser" γ-NiOOH phase in seawater compared to pure water. Relying solely on Raman peak intensity ratios to determine phase density is highly speculative, as these intensities are strongly influenced by surface roughness, laser focus, and sample orientation. Additional direct structural evidence, such as grazing-incidence XRD, is necessary to substantiate the claim of a denser structure.

Response: We sincerely thank the reviewer for this valuable comment. Regarding the suggestion of grazing-incidence XRD, we note that the reconstructed γ-NiFeOOH phase is predominantly amorphous. This is supported by the powder XRD results, which show no detectable diffraction peaks corresponding to γ-Ni(Fe)OOH (Supplementary Fig. S30). This observation is consistent with previous reports in the literature (e.g., *Angew. Chem. Int. Ed.* **60**, 26829–26836 (2021); *Nano Lett.* **23**, 5027–5034 (2023); *Appl. Catal. B-Environ.* **305**, 121033 (2022)). Therefore, XRD is unable to provide direct evidence for differences in structural compactness or density.

Instead, our conclusion regarding the formation of a denser γ-NiFeOOH phase in

alkaline seawater is primarily based on EXAFS analysis, which directly probes the local bond lengths distances. As shown in Fig. 3b–3d and Table S2, the Ni–Fe bond length distance decreases from 3.15 Å in alkaline water to 2.93 Å in alkaline seawater, providing clear quantitative evidence for the formation of a more compact oxyhydroxide phase. The correlation of shortened metal–metal bond distances in EXAFS spectra with the activation of the OPM pathway is consistent with literature reports (*J. Am. Chem. Soc.* **145**, 7829–7836 (2023); *Angew. Chem. Int. Ed.* e8854134 (2026); *Appl. Catal. B: Environ.* **354**, 124114 (2024); *Adv. Mater.* **38**, e72241 (2026); *J. Am. Chem. Soc.* **147**, 34169–34180 (2025); *Adv. Funct. Mater.* **36**, e16646 (2026)).

Furthermore, the Raman $I_{\delta/\nu}$ ratio is used only as complementary evidence to support the EXAFS-observed bond length contraction. The $I_{\delta/\nu}$ ratio is positively correlated with the structural looseness of NiOOH (e.g., *Appl. Catal. B: Environ.* **342**, 123376 (2024); *J. Phys. Chem. C* **119**, 7243–7254 (2015); *Nat. Commun.* **16**, 6624 (2025); *Energy Environ. Sci.* **17**, 1468–1481 (2024); *Adv. Funct. Mater.* **36**, e23847 (2026)). Therefore, the lower $I_{\delta/\nu}$ ratio observed in alkaline seawater suggests the formation of a denser γ-NiFeOOH structure, which is consistent with the EXAFS results.

3. Long-term Stability of the Protective Layer: Regarding the S 2p XPS analysis (Figure 1e), the authors assign peaks to M-S and S-O bonds. For a catalyst operating over 7000 hours, it is critical to understand the long-term stability of this sulfur species. Does the sulfide completely oxidize to dissolved sulfate over time? If so, how is the chloride-repelling layer maintained during the 7000-hour test. XPS spectra for the S 2p region after the 7000-hour test must be provided and discussed.

Response: We sincerely thank the reviewer for this insightful comment. To address the long-term stability of the sulfur species, we performed XPS analysis on the NiFe-MOF-S catalyst after 7000 hours of operation at 1.0 A cm^{-2} in alkaline seawater. As shown in Supplementary Fig. S32, the S 2p spectrum of the catalyst after 7000 h of operation clearly exhibits characteristic peaks corresponding to S–O and M–S bonds. This result indicates that the original NiS_2 nanoparticles undergo partial oxidation to surface-bound

sulfate species during the initial stage of electrolysis. These sulfate species subsequently remain stably anchored on the catalyst surface through coordination interactions with metal sites, even after 7000 h of operation. The co-existence of SO_4^{2-} species and NiS_2 ensures sustained Cl^--repelling capability. Specifically, the surface-bound SO_4^{2-} species provide electrostatic repulsion toward Cl^-, while the remaining NiS_2 can continuously generate sulfate species during operation, thereby replenishing and maintaining the protective layer over time. This mechanism explains how the chloride-repelling layer can be maintained during prolonged operation over 7000 h. This observation is consistent with recent reports in which surface-bound sulfate species remained detectable by XPS even after thousands of hours of electrolysis, further confirming that SO_4^{2-} can be stably anchored through coordination interactions with metal sites (e.g., *Nat. Commun.* **17**, 3014 (2026); *Adv. Funct. Mater.* **35**, 2419871 (2025); *Appl. Catal. B: Environ. Energy* **381**, 125897 (2026)). Furthermore, the sustained presence of the SO_4^{2-} protective layer may be attributed to the directional migration and preferential adsorption of SO_4^{2-} species onto the anode surface under the applied electric field. In addition, the high chemical and electrochemical stability of SO_4^{2-} makes it resistant to oxidation under anodic operating potentials, thereby contributing to its long-term stability (e.g., *Angew. Chem. Int. Ed.* **60**, 22740–22744 (2021)). We have included this new XPS data and added related discussion in the revised manuscript (line 231 of page 13 to line 235 of page 14).

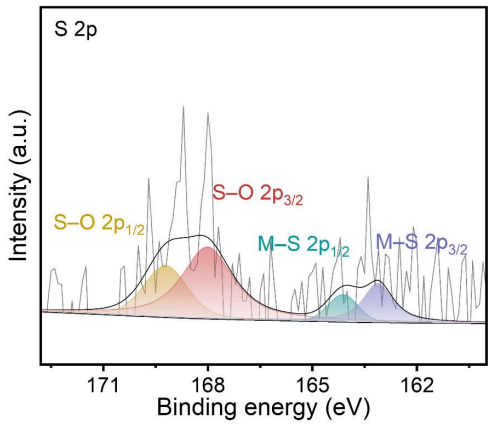

Fig. S32. XPS spectrum of S 2p for NiFe-MOF-S after 7000-h durability test at 1.0 A

cm^{-2} in 1 M KOH + seawater.

4. The author said that "the SEM images of NiFe-MOF-S/NF confirm that both the crystal structure and petal-like morphology of NiFe-MOF-S/NF are well preserved after long-term operation", but this structure is no longer visible in Figure S28. The author should have been more precise in your description in the text.

Response: We sincerely thank the reviewer for pointing out this inadequate description. After long-term operation, the original petal-like nanosheet morphology is no longer observed. Instead, the surface becomes rougher and only a flake-like morphology is retained (Supplementary Fig. S31), indicating the structural transformation of MOFs to the γ-NiFeOOH layer. The relevant text has been revised in the manuscript to more accurately describe the observed structural evolution (lines 229–231 of page 13).

5. The font size and style in each figure of the text should be made more uniform, for example, in Figure 2f.

Response: We sincerely thank the reviewer for this valuable suggestion. We sincerely apologize for these oversights. We have carefully revised all figures in the manuscript to ensure consistency in font size and style.

Responses to reviewer #3:

This manuscript reports a chloride-assisted catalyst reconstruction strategy to enhance activity and durability for alkaline seawater electrolysis using NiFe-MOF-derived catalysts. The authors demonstrate that trace amounts of Cl^- promote the formation of a dense γ-NiFeOOH phase, leading to improved OER activity and stability even at industrially relevant current densities. The work combines electrochemical measurements, operando spectroscopy, and DFT calculations, and the reported performance (e.g., 1.0 A cm^{-2} over 7000 h) is highly impressive. Overall, the topic is timely and important, and the combination of mechanistic insight (Fig. 3–4) and device-level demonstration (Fig. 5) makes the work potentially impactful. However, several key issues related to data interpretation, clarity of electrochemical analysis, and mechanistic justification need to be addressed before the manuscript can be considered for publication. I therefore recommend major revision.

Response: We sincerely thank the reviewer for the positive recommendation and the high evaluation of our work. We also greatly appreciate the constructive comments and suggestions regarding data interpretation, the clarity of the electrochemical analysis, and the mechanistic justification. These comments have greatly helped us improve the quality and clarity of the manuscript. All issues raised by the reviewer have been carefully addressed in the revised manuscript, as detailed in the point-by-point responses provided below.

Major comments

1. Unclear origin of Cl^--induced activity enhancement in single-metal systems

The authors report that even single-metal systems (Ni-MOF, Fe-MOF) show improved activity with increasing Cl^- concentration (page 7, lines 115–125). However the explanation for this phenomenon is insufficient and largely speculative. The proposed mechanism based on dual-site regulation does not apply to single-metal systems. Fig. S4 does not clearly support the claimed trend, and the data presentation is not sufficiently clear to validate this conclusion.

Recommendation: Provide a clearer mechanistic explanation specifically for single-metal systems.

Include additional control experiments or discussion (e.g., surface reconstruction, conductivity, double-layer effects).

Improve clarity and readability of Fig. S4 (especially panel a and c).

Response: We sincerely thank the reviewer for the valuable suggestion. We performed additional electrochemical measurements on Ni-MOF/NF and Fe-MOF/NF over a range of Cl^- concentrations. Similar to NiFe-MOF/NF, both Ni-MOF/NF and Fe-MOF/NF exhibit a volcano-shaped dependence of OER activity on Cl^- concentration, with optimal performance achieved at 0.05 M NaCl (Supplementary Fig. S5). Excessive Cl^- concentrations (>0.05 M) lead to significant activity suppression of OER activity due to corrosion effects, consistent with the behavior observed in the dual-metal system.

Furthermore, CV analysis shows that at a low Cl^- concentration (0.05 M), both Ni-MOF/NF and Fe-MOF/NF exhibit higher reduction peak currents compared with Cl^--free conditions (Supplementary Figs. S46 and S47). In contrast, at 0.5 M Cl^-, both catalysts exhibit lower reduction peak currents, owing to excessive Cl^--induced corrosion. These results are consistent with those observed for bimetallic system, indicating that trace of Cl^- promotes surface reconstruction of both single- metal and bimetallic MOFs into active oxyhydroxide phases for OER. The new results for the single-metal systems have been included as Figures S5, S46, and S47, and the corresponding discussion has been incorporated into the revised manuscript (lines 117–119 of page 7 and lines 328–332 of page 19).

In addition, as suggested by the reviewer, we have improved the clarity and readability of Fig. S4.

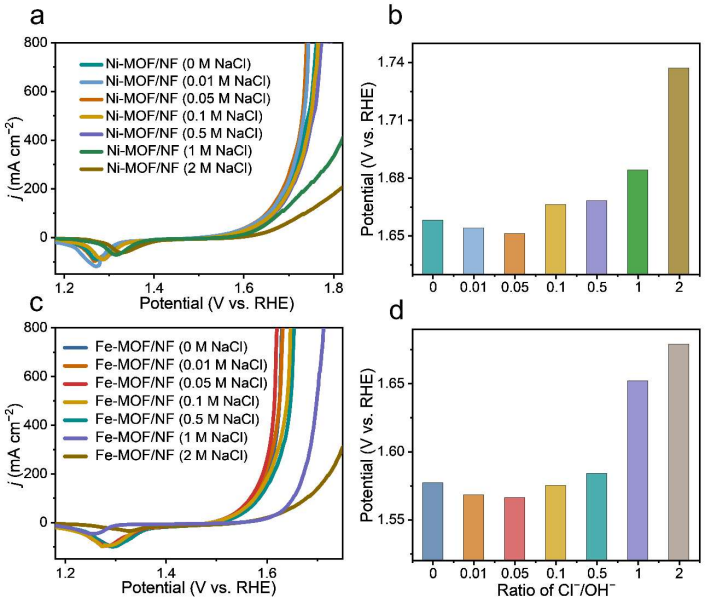

Fig. S5. (a, c) The LSV polarization curves for (a) Ni-MOF/NF and (c) Fe-MOF/NF in electrolytes with different Cl^-/OH^- ratios in 1 M KOH. (b, d) Comparison of overpotentials for (b) Ni-MOF/NF and (d) Fe-MOF/NF at a current density of 100 mA cm^{-2}.

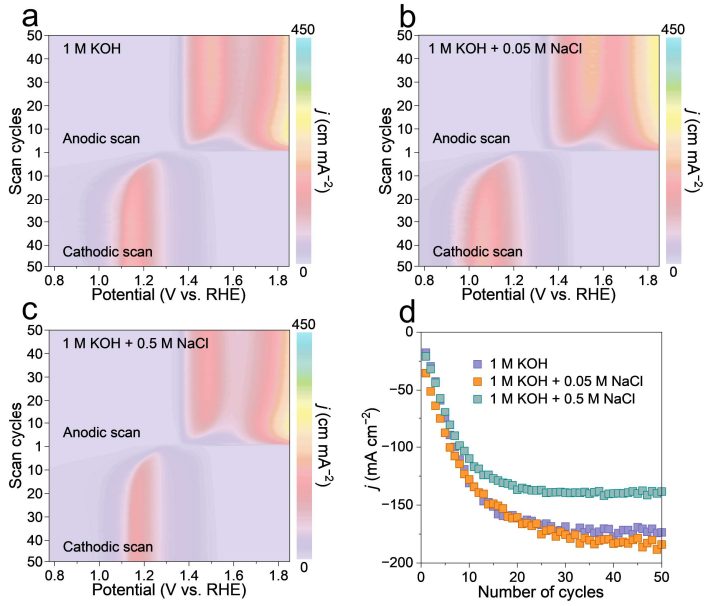

Fig. S46. (a, b, c) The evolution of CV curves for Ni-MOF/NF from the 1st to the 50th cycle in (a) 1 M KOH, (b) 1 M KOH + 0.05 M NaCl, and (c) 1 M KOH + 0.5 M NaCl at 20 mV s^{-1} between 0.774 and 1.85 V vs. RHE. (d) The variation of reduction peak

current density with CV cycles for Ni-MOF/NF in 1 M KOH, 1 M KOH + 0.05 M NaCl, and 1 M KOH + 0.5 M NaCl.

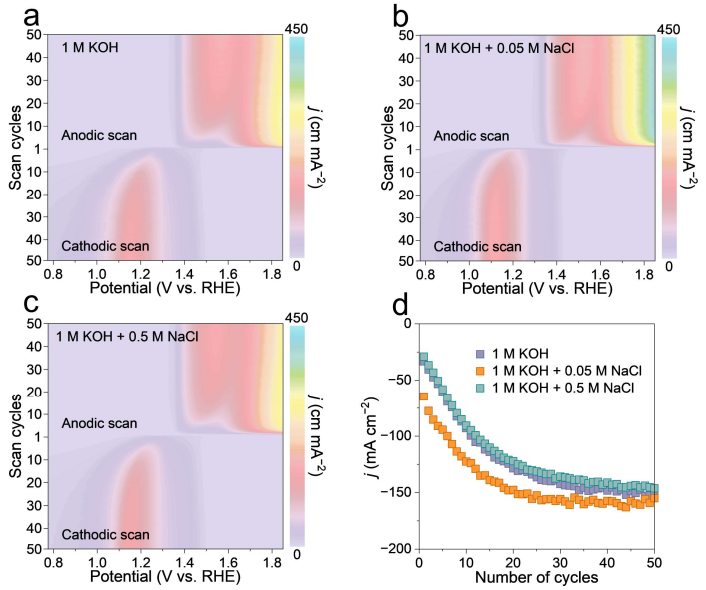

Fig. S47. (a, b, c) The evolution of CV curves for Fe-MOF/NF from the 1st to the 50th cycle in (a) 1 M KOH, (b) 1 M KOH + 0.05 M NaCl, and (c) 1 M KOH + 0.5 M NaCl at 20 mV s^{-1} between 0.774 and 1.85 V vs. RHE. (d) The variation of reduction peak current density with CV cycles for Fe-MOF/NF in 1 M KOH, 1 M KOH + 0.05 M NaCl, and 1 M KOH + 0.5 M NaCl.

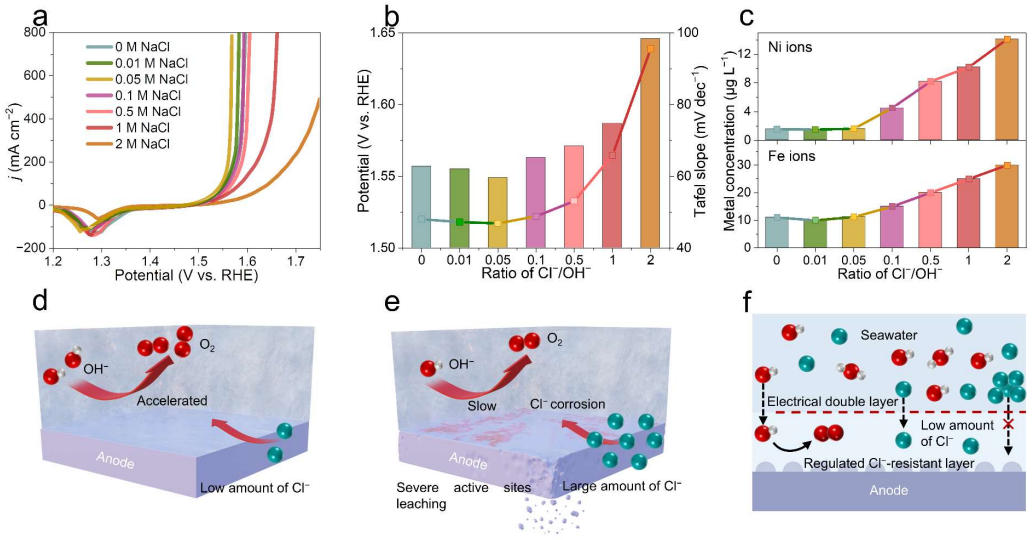

Fig. S4. Effect of Cl^- concentration on OER performance. (a) The LSV polarization

curves for NiFe-MOF/NF in electrolytes with different Cl^-/OH^- ratios in 1 M KOH. (b) Comparison of Tafel slopes and overpotentials at a current density of 100 mA cm^{-2}. (c) The dissolution concentrations of Ni ions and Fe ions during CP tests for 24 hours in different electrolytes. (d, e) The schematic diagram of Cl^- effect with (d) low and (e) large amount of Cl^-/OH^- ratios in 1 M KOH. (f) The proposed strategy to utilize traces of Cl^- to promote OER performance in seawater electrolysis.

2. Ambiguous peak assignment and spectroscopic interpretation

There are multiple issues regarding peak assignment: The assignments in page 9 (lines 139–140) are vague and lack justification. In the discussion around pages corresponding to lines 156–158, it is unclear which peaks are being referred to. Similar ambiguity appears in Raman/XAS discussions (Fig. 3 and related supplementary figures). These issues reduce confidence in the mechanistic conclusions.

Recommendation: Clearly indicate which peaks correspond to which chemical species in all figures.

Provide references or fitting details for peak assignments. Ensure consistency between main text and supplementary figures.

Response: We sincerely thank the reviewer for this valuable comment. We have assigned the characteristic peaks in both Raman spectra and XAFS spectra. For the Raman spectra shown in Fig. 1d, the peaks located at 270, 283, and 485 cm^{-1} are assigned to T_g, E_g, and A_g modes of NiS_2, respectively (e.g., *Phys. Rev. B* **84**, 235134 (2011); *J. Am. Chem. Soc.* **144**, 6028–6039 (2022); *J. Energy Chem.* **84**, 112–121 (2023); *Angew. Chem. Int. Ed.* **64**, e202511112 (2025); *Angew. Chem. Int. Ed.* **59**, 22470–22474 (2020)). These peak assignments confirm the presence of NiS_2 species in NiFe-MOF-S. The corresponding text and figure caption have been revised to include these detailed peak assignments, and the spectral presentation in Fig. 1d has been improved to enhance clarity (lines 139–141 of page 9).

For the XAFS spectra, enlarged views highlighting the absorption edge positions have been added to the revised Supplementary Figs. S11 and S12 to provide clearer

visualization. The Ni K-edge XANES spectrum of NiFe-MOF-S closely resembles that of NiO, indicating that Ni predominantly exists in the +2 oxidation state (Supplementary Fig. S11). The Fe K-edge XANES spectrum of NiFe-MOF-S exhibits an absorption edge position similar to that of Fe_2O_3, confirming that Fe predominantly exists in the +3 oxidation state (Supplementary Fig. S12). These assignments provide a reliable basis for understanding the electronic structure of the catalyst prior to reconstruction. The corresponding discussion has also been incorporated into the revised manuscript (lines 160–165 of page 10).

Additionally, we have addressed the ambiguity in FTIR spectral assignments (Supplementary Fig. S7). For both samples, the absorption band at approximately 540 cm^{-1} is assigned to M–O vibrations, the band at 748 cm^{-1} corresponds to C–H bending vibrations, and the band at 820 cm^{-1} is attributed to M–OH vibrations (e.g., *Adv. Funct. Mater.* **31**, 2102066 (2021); *J. Colloid Interface Sci.* **678**, 795–805 (2025); *Adv. Funct. Mater.* **34**, 2408823 (2024)). The absorption band at approximately 600 cm^{-1} is assigned to Ni–S vibrations, which is consistent with recent reports on metal–sulfur coordination in similar systems (e.g., *Nat. Commun.* **17**, 3014 (2026); *J. Energy Chem.* **84**, 112–121 (2023); *J. Colloid Interf. Sci.* **617**, 620–632 (2022); *Adv. Funct. Mater.* **36**, e28665 (2026)). This assignment further confirms the presence of NiS_2 species in the catalyst and is consistent with the Raman and XPS results. These peak assignments have been added to the revised manuscript (lines 141–146 of page 9).

To clarify the peak assignments during the reconstruction process, we have included the XAS data of the pristine catalyst (before OER) together with the post-OER data in Fig. 3a–3c. The Ni K-edge XANES spectrum of NiFe-MOF-S shows that the absorption edge position closely resembles that of NiO (Fig. 3a). After the OER test, the Ni and Fe K-edges XANES spectra of the post-OER NiFe-MOF-S shift toward higher energies relative to those of the pristine catalyst, indicating increased oxidation states after reconstruction. Importantly, the Ni–M (Fe–M) bond distances decrease from 3.13 Å (3.15 Å) in alkaline water to 2.93 Å (2.96 Å) in alkaline seawater, indicating the formation of a more compact metal oxyhydroxide phase with shortened Ni–Fe bonds

under alkaline seawater conditions (Fig. 3b, 3c, and Supplementary Table S2). The revised Figures and the corresponding discussion have been updated accordingly in the manuscript (lines 290–293 of page 17 and lines 354–360 of page 20).

Furthermore, in situ Raman spectroscopy shows that a peak at 480 cm^{-1} appears in both alkaline water and alkaline seawater at low potentials beginning at 1.25 V, which is assigned to the bending vibration of Ni^{2+}–O in $Ni(OH)_2$ (e.g., *ACS Nano* **18**, 20459–20467 (2024); *Angew. Chem. Int. Ed.* **64**, e202502151 (2025); *Angew. Chem. Int. Ed.* e9878440, (2026). doi.org/10.1002/anie.9878440). As the potential further increases, new peaks emerge at 475 and 555 cm^{-1}, which are assigned to the bending (δ(Ni–O)) and stretching (ν(Ni–O)) vibrations of Ni^{3+}–O species in NiOOH, respectively (Fig. 3k, 3l, and Supplementary Fig. S49) (e.g., *J. Am. Chem. Soc.* **147**,1334–1343 (2025); *Angew. Chem. Int. Ed.* 64, e202510741 (2025)). We have updated the revised figures and added related discussion in the revised manuscript (lines 342–344 of page 20).

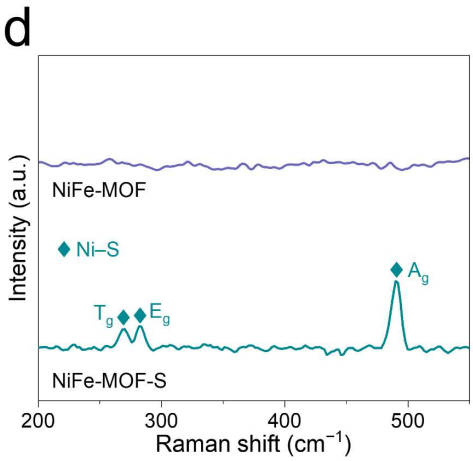

Fig. 1. (d) Raman spectra of NiFe-MOF and NiFe-MOF-S detached from the NF substrate.

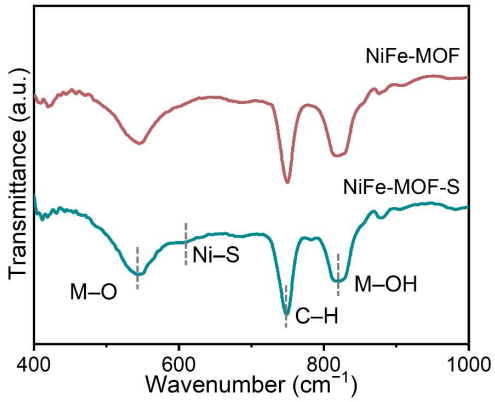

Fig. S7. FTIR spectra of NiFe-MOF and NiFe-MOF-S detached from the NF substrate.

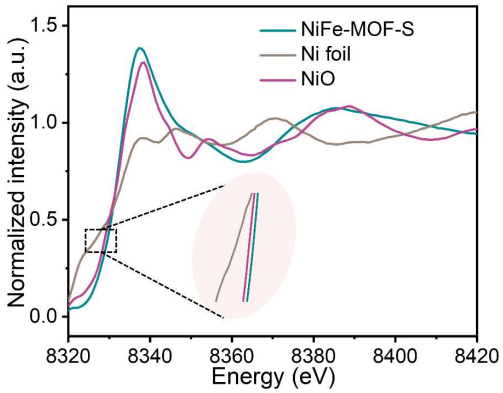

Fig. S11. Ni K-edge XANES spectra of Ni foil, NiO, and NiFe-MOF-S detached from the NF substrate.

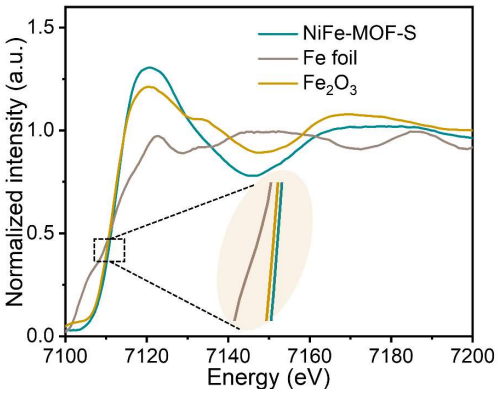

Fig. S12. Fe K-edge XANES spectra of Fe foil, Fe_2O_3, and NiFe-MOF-S detached from the NF substrate.

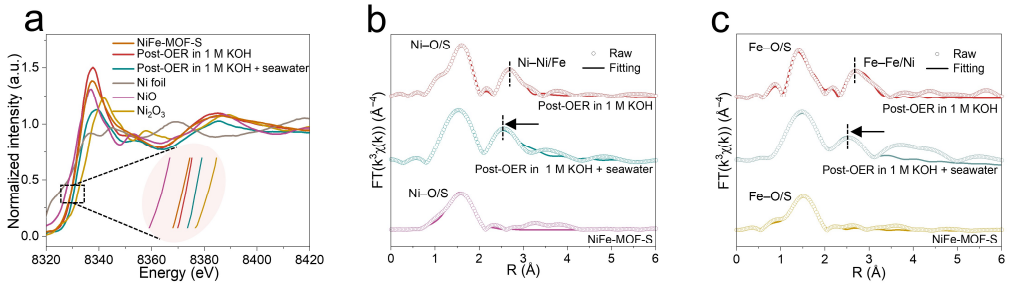

Fig. 3. (a) Ni K-edge XANES spectra of NiFe-MOF-S and post-OER NiFe-MOF-S in alkaline water and alkaline seawater. (b) Ni K-edge FT EXAFS fitting curves of NiFe-MOF-S and post-OER NiFe-MOF-S in alkaline water and alkaline seawater. (c) Fe K-edge FT EXAFS fitting curves of NiFe-MOF-S and post-OER NiFe-MOF-S in alkaline water and alkaline seawater.

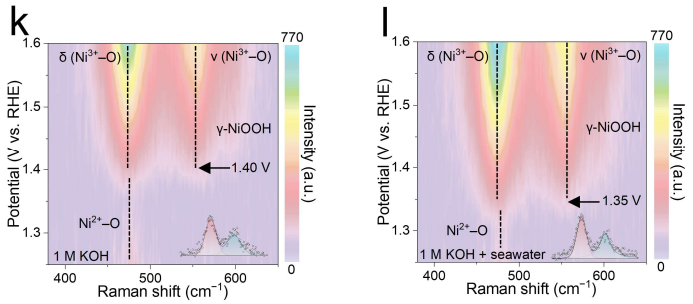

Fig. 3. (k, l) Potential-dependent in-situ Raman spectra in (k) alkaline water and (l) alkaline seawater during the OER process.

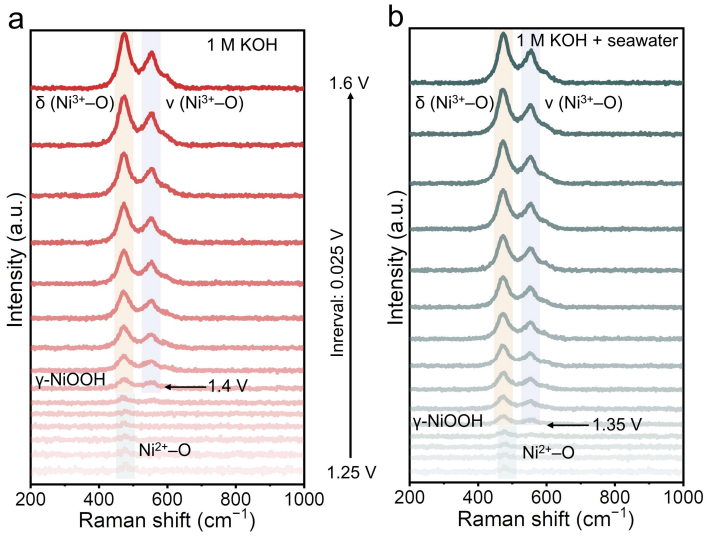

Fig. S49. Potential-dependent in-situ Raman spectra during the OER process in (a) 1

M KOH and (b) 1 M KOH + seawater.

3. Inconsistency and insufficient explanation in LSV measurements

The manuscript states that LSV was measured at 5 mV s^{-1}, but the presence of reduction peaks (e.g., Fig. 2a) suggests that scans may have been performed in the negative direction (−5 mV s^{-1}). The origin of the reduction peaks is not explained when first introduced. The relationship between these peaks and catalyst reconstruction (Fig. 3j) is not clearly discussed.

Recommendation: Clarify scan direction and measurement protocol. Explicitly assign the reduction peaks (e.g., Ni^{2+}/Ni^{3+} redox). Discuss how peak intensity relates to catalyst reconstruction and activity.

Response: We sincerely thank the reviewer for pointing out this mistake. The LSV measurements were conducted in the negative scan direction at a scan rate of −5 mV s^{-1}. The description of the scan direction has been corrected accordingly in the Materials and Methods section (lines 630–631 of page 35).

To explicitly identify the redox features, we have added labels corresponding to the Ni^{2+}/Ni^{3+} oxidation process in the CV curves shown in Fig. 3g and 3h. The reduction peak corresponds to the reduction of Ni^{3+} back to Ni^{2+}, and its intensity is directly related to the amount of electrochemically active Ni^{3+} species generated during the anodic scan. The reduction peak current of NiFe-MOF-S/NF is significantly larger in alkaline seawater than in alkaline water, indicating that Cl^- promotes the formation of electrochemically active Ni^{3+} species (Fig. 3j).

To further support the correlation between the Ni^{2+}/Ni^{3+} redox behavior and OER activity, we correlated the reduction peak current density with the potential required to achieve 100 mA cm^{-2} for NiFe-MOF-S/NF in both alkaline water and alkaline seawater (Supplementary Fig. S44). As the number of CV cycles increases, the reduction peak current density gradually increases, while the corresponding potential required to achieve 100 mA cm^{-2} correspondingly decreases. In alkaline seawater, the reduction peak current densities are consistently higher, while the potentials required to achieve

100 mA cm^{-2} are lower than those in alkaline water. These results indicate that Cl^- promotes the formation of a greater number of Ni^{3+} active sites and enhances OER kinetics. This relationship further confirms that the Cl^--induced generation of Ni^{3+} species directly contributes to the enhanced OER activity. These clarifications and peak assignments have been incorporated into the revised manuscript (line 318 of page 18 to line 328 of page 19).

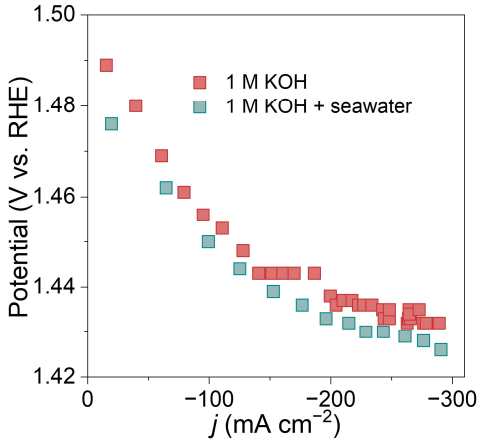

Fig. S44. Correlation between reduction peak current densities and the potential required to reach a current density of 100 mA cm^{-2} for NiFe-MOF-S/NF in alkaline water and alkaline seawater. The x-axis represents the reduction peak current densities extracted from the CV curves. The y-axis represents the potential required to reach a current density of 100 mA cm^{-2}.

4. Insufficient treatment of error analysis and reproducibility

Error bars are missing or insufficiently described (e.g., Fig. 2c). There is no clear indication of repeatability or statistical variation.

Recommendation: Include error bars for key electrochemical data. Provide number of replicates and standard deviations. Clarify whether the presented data are representative or averaged.

Response: We sincerely thank the reviewer for this important and insightful comment. To address the reviewer's concerns regarding error analysis and reproducibility, we have added error bars to Fig. 2c (Arrhenius plot), representing the standard deviation

obtained from three independent measurements. These revisions have been incorporated into the updated Fig. 2c and the corresponding discussion in the main text (lines 201–204 of page 12).

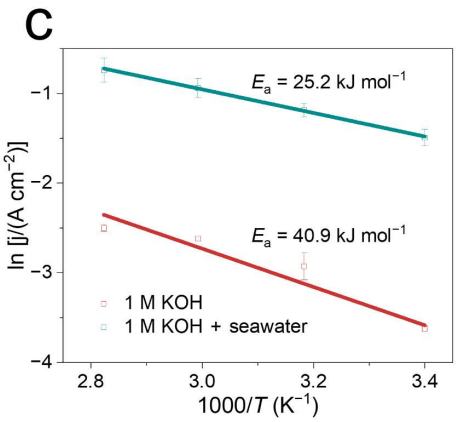

Fig. 2. (c) Arrhenius plot of NiFe-MOF-S/NF at 1.4 V vs. RHE in 1 M KOH and (b) 1 M KOH + seawater.

5. Questionable analysis of degradation rate (1.4 μV h^{-1})

The authors claim an ultralow degradation rate of 1.4 μV h^{-1} based on Fig. 2d/i. However, the potential profile clearly fluctuates over time. It is unclear how this value was extracted.

Given the noise level, the significance of 1.4 μV h^{-1} is questionable.

Recommendation: Provide a detailed method for calculating degradation rate (e.g., linear fitting window). Include statistical uncertainty. Discuss whether the fluctuation level allows meaningful extraction of such a small value.

Response: We sincerely thank the reviewer for the valuable comment. This degradation rate calculation method is consistent with previous reports (e.g., *Nat. Commun.* **14**, 3607 (2023); *Adv. Mater.* **36**, 2408982 (2024); *Adv. Energy Mater.* **16**, e05239 (2026); *Nat. Commun.* (2026). https://doi.org/10.1038/s41467-026-71943-6) and is based on the following equation: decay voltage (D_V) = (V_2 – V_1)/t, where V_1 and V_2 are the average potential over the first 10% and last 10% of the operation period, respectively, and t denotes the total operation time. The degradation rate was calculated as follows:

the potential values were averaged over the first 10% of the operation period (the initial 700 h) and the last 10% of the operation period (the final 700 h). The average potential during the first 700 h was 2.08825 V vs. RHE, whereas that during the last 700 h was 2.09819 V vs. RHE. The difference between these two average values was 9.94 mV. Dividing this potential difference by the total operation time of 7000 h yields a degradation rate of 1.42 μV h^{-1}, which is rounded to 1.4 μV h^{-1}. This value is comparable with previous reports (*Nat. Commun.* **14**, 3607 (2023)), *Adv. Mater.* **36**, 2408982 (2024), *Adv. Energy Mater.* **16**, e05239 (2026)). Furthermore, this value is lower than the technical target of 2.3 μV h^{-1} established by the United States Department of Energy for 2026. This calculation method has been added to the revised manuscript (lines 656–658 of page 36).

6. Insufficient evidence for correlation between Cl^- concentration, reduction peak, and activity

In Fig. 3, the authors suggest a correlation between: Cl^- concentration, Reduction peak intensity, and OER activity. However, no quantitative correlation analysis is provided. The causality remains unclear.

Recommendation: Provide quantitative correlation (e.g., peak current vs activity). Consider additional experiments (e.g., controlled CV cycles, operando tracking).

Response: We sincerely thank the reviewer for this valuable suggestion. To establish a clearer correlation among Cl^- concentration, reduction peak intensity, and OER activity, we performed additional CV measurements on NiFe-MOF-S/NF in electrolytes containing different Cl^- concentrations (1 M KOH + 0.05 M NaCl, 1 M KOH + 0.1 M NaCl, and 1 M KOH + 0.5 M NaCl) (Supplementary Fig. S45).

Compared with the Cl^--free electrolyte (1 M KOH), the Cl^--containing electrolytes exhibit a lower onset potential for Ni^{2+} oxidation and a significantly higher reduction peak current density. Moreover, the reduction peak current progressively increases as the Cl^- concentration rises from 0.05 M to 0.5 M NaCl (Supplementary Fig. S45a–c), indicating that a higher Cl^- concentrations promote the generation of a greater amount

of oxidizable Ni^{2+} species. Furthermore, we directly correlated the reduction peak current density with the potential required to achieve 100 mA cm^{-2} under different Cl^- concentrations (Supplementary Fig. S45d). The results show that, as the Cl^- concentration increases from 0 to 0.5 M, the reduction peak current density gradually increases, whereas the potential required to achieve 100 mA cm^{-2} correspondingly decreases. Thus, a clear Cl^- concentration-dependent relationship is observed, in which higher Cl^- concentrations lead to larger reduction peak currents and lower overpotentials. This provides quantitative evidence that Cl^- promotes catalyst reconstruction and enhances OER kinetics in a concentration-dependent manner. These results provide direct quantitative evidence linking Cl^- concentration with the increased formation of active Ni^{3+} species, as reflected by the reduction peak current, and the corresponding enhancement in OER activity. This analysis has been incorporated into the revised manuscript (lines 322–328 of page 19).

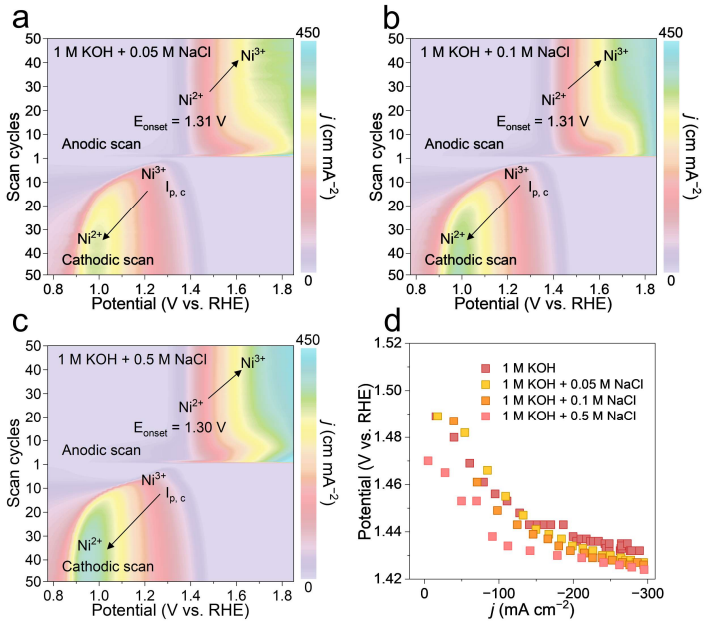

Fig. S45. (a–c) The evolution of CV curves for NiFe-MOF-S/NF from the 1st to the 50th cycle in (a) 1 M KOH + 0.05 M NaCl, (b) 1 M KOH + 0.1 M NaCl, and (c) 1 M KOH + 0.5 M NaCl at 20 mV s^{-1} between 0.774 and 1.85 V vs. RHE. (d) Correlation between reduction peak current densities and the potential required to reach a current density of 100 mA cm^{-2} for NiFe-MOF-S/NF in 1 M KOH, 1 M KOH + 0.05 M NaCl, 1 M KOH

+ 0.1 M NaCl, and 1 M KOH + 0.5 M NaCl. The x-axis represents the reduction peak current densities extracted from the CV curves. The y-axis represents the potential required to reach a current density of 100 mA cm^{-2}.

Finally, the mechanistic insight (Fig. 4) and performance (Fig. 5) are highly significant and could make this work suitable for publication in a high-impact journal. However, the current manuscript contains several issues in data interpretation, electrochemical analysis, and clarity.

I recommend publication after major revision addressing the points above.

Response: We sincerely thank the reviewer for the positive evaluation of our work, particularly for recognizing the significance of the mechanistic insights and the performance achieved in this study. We appreciate the reviewer's constructive comments regarding data interpretation, electrochemical analysis, and presentation clarity, which have greatly helped us to improve the manuscript. All the issues raised by the reviewer have been carefully addressed in the revised version. We hope that the revised manuscript now meets the standards required for publication.

Responses to reviewer #4:

This work proposes a strategy to regulate the flux of chloride ions near the catalytic sites during seawater electrolysis. Sulfur species generate sulfate in situ to repel most Cl^- while allowing a small amount of chloride to remain and promote catalyst reconstruction. As a result, the catalyst reconstructs into a dense γ-NiFeOOH phase with shortened Ni–Fe bond lengths, which improves the OER activity and stability in alkaline seawater. A series of electrochemical measurements and operando characterizations are provided to support the proposed mechanism. Some technical issues need to be addressed before further consideration of this work.

Response: We sincerely thank the reviewer for the positive recommendation of our work and for the constructive comments and suggestions. These insightful remarks have helped us improve the clarity, rigor, and overall quality of the manuscript. We have carefully revised the manuscript and provided detailed point-by-point responses below.

1. The structural description of the catalyst needs clarification. The manuscript refers to sulfur-doped NiFe nanoparticles, while Fig. 1 suggests the formation of NiS_2 nanoparticles. It should be clarified whether sulfur is present as dopants or forms a separate sulfide phase.

Response: We sincerely thank the reviewer for this valuable comment. We agree that the original description could lead to ambiguity regarding the role of sulfur in the catalyst structure. We would like to clarify that sulfur is not incorporated as a dopant within the NiFe lattice. Instead, sulfur exists in the form of discrete NiS_2 nanoparticles uniformly decorated on the surface of NiFe-MOF nanosheets. This conclusion is supported by multiple characterization results. Specifically, the XRD patterns exhibit characteristic diffraction peaks corresponding to NiS_2 (Fig. 1c), and the TEM images clearly reveal the presence of distinct NiS_2 nanoparticles distributed on the nanosheets (Fig. 1f). In addition, the XPS spectra display characteristic Ni–S bonding signals (Fig. 1e), further confirming the formation of a separated sulfide phase rather than sulfur doping. To avoid confusion, we have revised the manuscript throughout to consistently

describe the catalyst as "NiS_2 nanoparticles decorated on NiFe-MOF" (lines 22–23 of page 3 and lines 71–73 of page 5).

2. The structural analysis in Fig. 3 mainly focuses on the catalyst after the OER test. To clearly demonstrate the reconstruction process, a direct comparison between the catalyst before and after OER should be provided.

Response: We sincerely appreciate the reviewer's valuable suggestion. To more clearly elucidate the catalyst reconstruction process, we have now included comparative XAS and XPS analyses of the catalyst before and after OER test in the revised Fig. 3. For the pristine NiFe-MOF-S catalyst, the Ni 2p XPS spectrum exhibits peaks at 873.4 and 855.5 eV, corresponding to Ni^{2+} species. This result is consistent with the Ni K-edge XANES spectra, where the absorption edge closely resembles that of NiO reference. After the OER process, an obvious Ni^{3+} component emerges in the XPS spectra, indicating the oxidation of Ni^{2+} during the electrochemical reconstruction. Furthermore, both the Ni and Fe K-edges XANES spectra of post-OER NiFe-MOF-S shift towards higher energies compared with those of the pristine sample, demonstrating increased oxidation states after reconstruction. The FT-EXAFS results additionally reveal changes in local coordination environments, supporting the formation of the reconstructed γ-NiFeOOH phase during OER operation. These newly added comparisons provide direct evidence for the structural and electronic evolution of the catalyst during reconstruction. The revised Fig. 3 and the corresponding discussion have been updated in the revised manuscript (lines 354–360 of page 20).

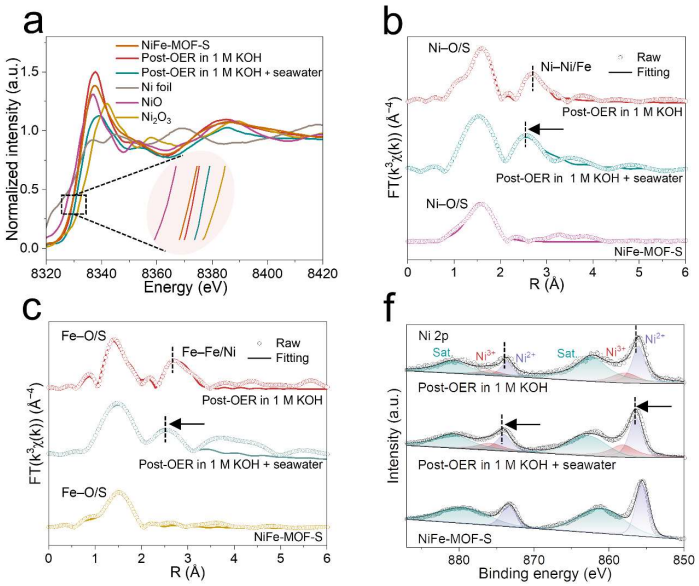

Fig. 3. (a) Ni K-edge XANES spectra of NiFe-MOF-S and post-OER NiFe-MOF-S in alkaline water and alkaline seawater. (b) Ni K-edge FT EXAFS fitting curves of NiFe-MOF-S and post-OER NiFe-MOF-S in alkaline water and alkaline seawater. (c) Fe K-edge FT EXAFS fitting curves of NiFe-MOF-S and post-OER NiFe-MOF-S in alkaline water and alkaline seawater. (f) XPS spectra of Ni 2p for NiFe-MOF-S and post-OER NiFe-MOF-S detached from the NF substrate.

3. The Raman data in Fig. 1d are not very convincing. The spectral quality is relatively poor, and the assignment of the additional peaks is too general, as they are simply attributed to M–S vibrations without sufficient explanation.

Response: We sincerely thank the reviewer for this valuable comment. We have remeasured and reprocessed the Raman spectra to improve the spectral quality, signal-to-noise ratio, and peak resolution. The characteristic Raman peaks located at 270, 283, and 485 cm^{-1} can now be clearly identified and are assigned to the T_g, E_g, and A_g vibrational modes of NiS_2, respectively. These assignments are supported by previous reports (e.g., *J. Am. Chem. Soc.* **144**, 6028–6039 (2022); *Angew. Chem. Int. Ed.* **64**, e202511112 (2025); *Angew. Chem. Int. Ed.* **59**, 22470–22474 (2020)). The improved Raman data therefore provide more convincing evidence for the successful formation

of NiS_2 species in NiFe-MOF-S catalyst. We have updated Fig. 1d and added related discussion in the revised main text (lines 139–141 of page 9).

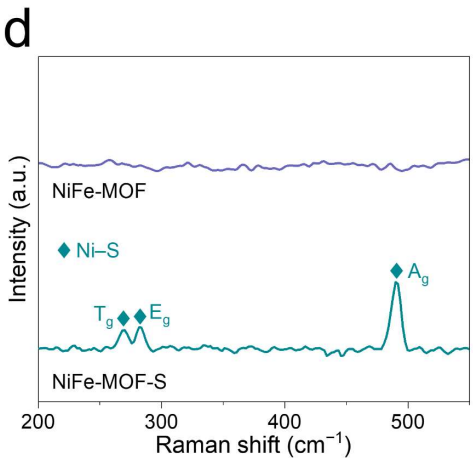

Fig. 1. (d) Raman spectra of NiFe-MOF and NiFe-MOF-S detached from the NF substrate.

4. Although the manuscript reports electrolyser performance, the experimental section does not include any description of the electrolyser testing.

Response: We sincerely thank the reviewer for pointing out this omission. To address this issue, we have added detailed descriptions of both the AEMWE and 1.0 kW ASWE testing procedures.

For AEMWE construction, NiFe-MOF-S/NF (geometric area: 1 cm^2) were employed as both anode and cathode, separated by an anion exchange membrane (1.2 × 1.2 cm^2) which were pretreated in 1 M KOH for over 24 h followed by thoroughly rinsed with water. The electrolyzer was operated using continuously circulated 30 wt% KOH + seawater electrolyte. The cell voltage was recorded without iR compensation. Long-term durability was evaluated at a constant current density of 2.0 A cm^{-2}.

For the 1.0 kW ASWE system, we additionally provided a detailed description of the scale-up synthesis procedure for the large-area NiFe-MOF-S/NF electrodes, including precursor composition, hydrothermal growth conditions, calcination, and sulfurization procedures. The assembled ASWE stack consisted of 13 cells with a total active anode

area of 1020.5 cm^2 (each cell: 78.5 cm^2). Commercial Raney Ni and a commercial diaphragm were used as the cathode and separator, respectively. The seawater electrolyte (30 wt% KOH + seawater) was pretreated to remove Mg/Ca precipitates by centrifugation before being circulated at 80 °C. Prior to tests, a leak check was performed to ensure no gas leakage in the system. The system pressure was kept constant at 0.1 M Pa during tests. The cell voltage was recorded without iR compensation. Long-term testing was performed at 0.5 A cm^{-2}.

To further improve clarity and reproducibility, we have also added optical photographs of the AEMWE electrolyzer (Supplementary Fig. S34) and the single-cell components of the ASWE system (Supplementary Fig. S65). The corresponding descriptions and figures have been added in the revised manuscript (lines 241–243 of page 14, lines 470–473 of page 28, and line 640 of page 35 to line 655 of page 36).

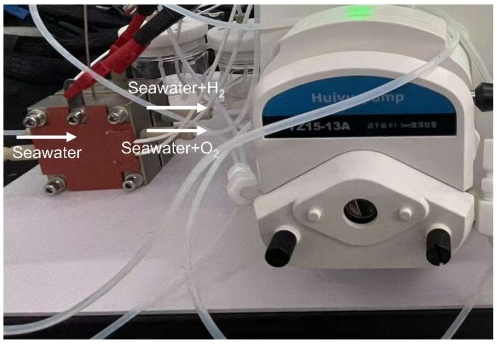

Figure S34. The optical photos of AEMWE electrolyzer.

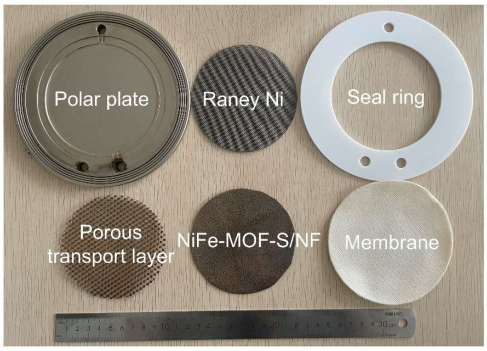

Fig. S65. Optical image for components included in a single cell.

5. The in situ ATR-SEIRAS spectra in Fig. 4a–b are not very convincing due to the

relatively weak signal intensity and poorly resolved spectral features.

Response: We sincerely appreciate the reviewer for the valuable comment. To improve the spectral quality and enhance the reliability of the spectral assignments, we reprocessed the in situ ATR-SEIRAS data by subtracting the background spectra collected at OCP. This treatment significantly improves the signal-to-noise ratio and the resolution of the characteristic bands. In the revised spectra, two common features are clearly observed in both alkaline water and alkaline seawater electrolytes. The broad band near 1155 cm^{-1} is assigned to SO_4^{2-} species generated from the oxidation of NiS_2 species, while the peak around 1265 cm^{-1} originated from Si–O–Si vibrations of the silicon substrate (e.g., *J. Am. Chem. Soc.* 145, 23659–23669 (2023); *Nat. Commun.* **16**, 3502 (2025)).

Importantly, distinct oxygen-intermediate-related features can now be clearly resolved under different electrolyte conditions. In alkaline seawater, a characteristic peak at 1104 cm^{-1} corresponding to the *O–O* stretching vibration is observed (Fig. 4a), which is attributed to the M–O–O–M intermediate associated with the OPM pathway (e.g., *Chem.* **7**, 2101–2117 (2021); *Nat. Catal.* **4**, 1012–1023 (2021); *J. Am. Chem. Soc.* **145**, 7829–7836 (2023)). By contrast, in alkaline water, a distinctive peak located at 1205 cm^{-1} is detected and assigned to *O–O intermediate involved in the LOM pathway. These improved spectra now provide clearer and more convincing evidence supporting the different OER mechanisms operating in alkaline water and alkaline seawater environments. The revised figures (as Fig. 4a and 4b) and the corresponding discussions have been updated in the manuscript (lines 409–410 of page 24).

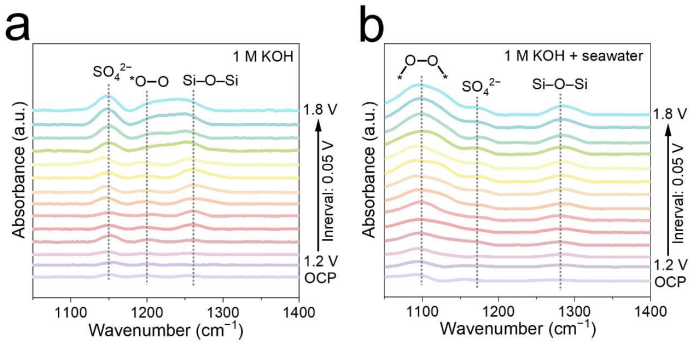

Fig. 4. (a, b) ATR-SEIRAS spectra recorded in the potential range of OCP and 1.2–1.8 V vs. RHE for NiFe-MOF-S/NF in (a) alkaline water and (b) alkaline seawater.

6. The authors should provide more details regarding the industrial electrolyzer tests. In particular, post-test characterization of the electrodes (e.g., morphology and structural analysis) is needed to explain the excellent stability observed during long-term operation.

Response: We sincerely thank the reviewer for this valuable suggestion. We have provided additional details regarding the industrial electrolyzer tests. For the large-area electrodes used in the 1.0 kW ASWE, NiFe-MOF-S/NF was synthesized using the same procedure as that employed for the laboratory-scale samples. Briefly, 1.0 g of $FeCl_3 \cdot 6H_2O$, 0.88 g of $NiCl_2 \cdot 6H_2O$, and 2.48 g of terephthalic acid were dissolved in 272 mL of a mixed solvent composed of DMF, ethanol, and distilled water. The solution was transferred into a Teflon-lined stainless-steel autoclave containing a circular Ni foam substrate with a diameter of 10 cm and subsequently heated at 120 °C for 12 h. After cooling, the sample was thoroughly rinsed, dried, and subsequently calcined at 300 °C under N_2 atmosphere for 2 h. Subsequent sulfide deposition was performed using sulfur powder at 300 °C for 2 h under an N_2 atmosphere, yielding large-area NiFe-MOF-S/NF electrodes for the 1.0 kW ASWE system.

For the 1.0 kW ASWE system, the stack consisted of 13 cells with a total active anode area of 1020.5 cm^2, corresponding to an active area of 78.5 cm^2 per cell. NiFe-MOF-S/NF was employed as the anode, commercial Raney Ni was used as the cathode,

and a commercial diaphragm served as the separator. The electrolyte, consisting of 30 wt% KOH + seawater, was pretreated by centrifugation to remove Mg/Ca precipitates and subsequently circulated through the system at 80 °C. The performance of ASWE system evaluated using an electrolyte composed of 30 wt% KOH and seawater. The cell voltage was recorded without iR compensation, and long-term durability was evaluated at a constant current density of 0.5 A cm^{-2}. Prior to tests, leak checks were conducted to ensure the absence of gas leakage within the system. The system pressure was maintained at a constant value of 0.1 M Pa throughout the tests. The long-term durability data of the ASWE system were collected using the direct current power supply. To clarify the cell configuration used in the 1.0 kW-scale ASWE system, we have included an optical image showing the components of a single cell, including the polar plate, Raney Ni, seal ring, porous transport layer, membrane, and NiFe-MOF-S/NF (Supplementary Fig. S65). The system pressure remained stable at approximately 0.1 MPa throughout the 1500 h operation of the 1.0 kW-scale ASWE system, indicating that no significant flow channel clogging or gas accumulation occurred (Supplementary Fig. S66).

Furthermore, to explain the excellent stability observed during the long-term operation, we have provided post-test characterizations of the electrode after 1500-h of operation. SEM image of the post-test electrode shows that the NiFe-MOF-S/NF catalyst retains its flake-like morphology after operation (Supplementary Fig. S68). The XRD patterns display only the characteristic diffraction peaks of the NF substrate, with no display diffraction peaks corresponding to other crystalline phases (Supplementary Fig. S69). This result confirms that the catalyst was fully reconstructed into an amorphous γ-NiFeOOH phase after long-term operation. These post-test characterization results are consistent with those obtained after the 7000-hour stability test (Supplementary Figs. S30 and S31). These results collectively demonstrate the excellent morphological and structural stability of the catalyst under industrial operating conditions, thereby accounting for the outstanding long-term durability observed. These characterizations and the corresponding discussions have been

incorporated into the revised manuscript (lines 488–497 of page 29, line 547 of page 31 to line 556 of page 32, and lines 647–655 of page 36).

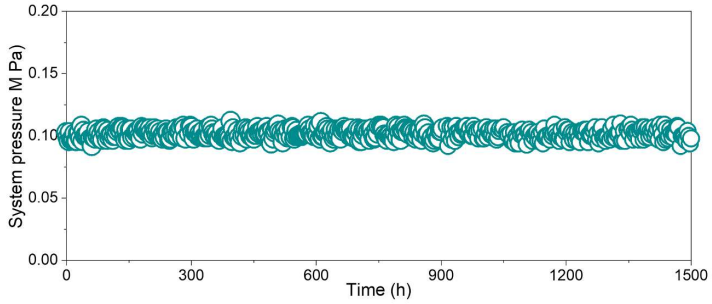

Fig. S66. System pressure of the 1.0 kW-scale ASWE for 1500-hour operation.

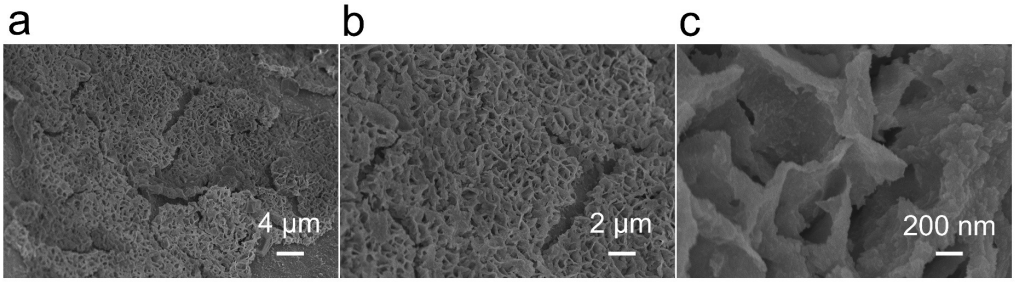

Fig. S68. SEM images of NiFe-MOF-S/NF after durability test in a 1.0 kW-scale ASWE.

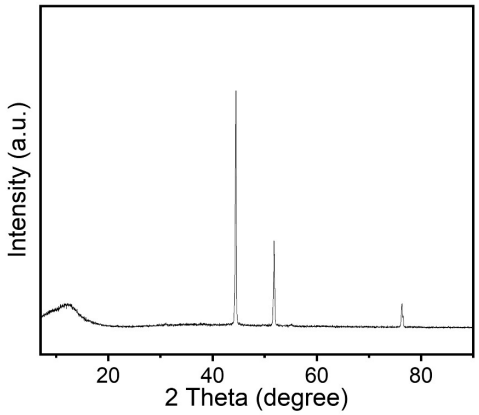

Fig. S69. XRD patterns of NiFe-MOF-S/NF after durability test in a 1.0 kW-scale ASWE.

7. The techno-economic analysis relies on several assumptions that are insufficiently justified, such as the electricity price (0.02 $/kWh), electrolyser capital cost (450 $/kW),

capacity factor (0.9), and catalyst/membrane cost (5% of electrolyser cost). These parameters appear overly optimistic and are not adequately supported by references.

Response: We sincerely thank the reviewer for this valuable comment. The parameters used in our techno-economic analysis were selected based on established literature reports. The electricity price of 0.02 $/kWh has been widely adopted in recent techno-economic studies (e.g., *Joule* **9**, 101968 (2025); *Sci. Adv.* **11**, eaea4543 (2025); *Nat. Mater.* **16**, 16–22 (2017)). The electrolyser capital cost of 450 $/kW is consistent with literature reports for low-cost electrolyzer systems (e.g., *Int. J. Hydrogen Energy* **48**, 32313–32330 (2023); *ACS Energy Lett*. **6**, 997–1002 (2021); *Catal. Sci. Technol.* **12**, 2912–2919 (2022)). Furthermore, the capacity factor (0.9) and the catalyst/membrane cost assumption (5% of the electrolyser cost) were adopted from previous studies (e.g., *Adv. Mater.* **37**, 2416658 (2025); *Angew. Chem., Int. Ed.* **63**, 202319936 (2024); *Nature* **617**, 724–729 (2023)).

Based on these assumptions, our calculated hydrogen production cost is \$1.66 kg^{-1}, which falls within the range of values reported in the literature (e.g., \$1.218 kg^{-1} in *Adv. Mater.* **37**, 2416658 (2025); \$1.702 kg^{-1} in *Nat. Commun.* **16**, 9261 (2025); \$1.74 kg^{-1} in *Adv. Mater.* **38**, e16751 (2026); \$1.81 kg^{-1} in *Adv. Mater.* **38**, e20960 (2026)), thereby confirming the reasonableness of the assumptions used in our analysis. Moreover, this value is lower than the 2026 target of \$2.0 kg^{-1} established by U.S. DOE, further demonstrating the economic competitiveness of our system. The corresponding references (Refs. 48–51) have been cited in the revised manuscript to support the techno-economic analysis.